

Two-channel Kondo physics in odd impurity chains

Andrew K. Mitchell,^{1,2} David E. Logan,¹ and H. R. Krishnamurthy³

¹*Department of Chemistry, Physical and Theoretical Chemistry, Oxford University, South Parks Road, Oxford OX1 3QZ, United Kingdom*

²*Institute for Theoretical Physics, University of Cologne, D-50937 Cologne, Germany*

³*Department of Physics, Indian Institute of Science, Bangalore 560 012, India*

(Received 30 March 2011; published 25 July 2011)

We study odd-membered chains of spin- $\frac{1}{2}$ impurities, with each end connected to its own metallic lead. For antiferromagnetic exchange coupling, universal two-channel Kondo (2CK) physics is shown to arise at low energies. Two overscreening mechanisms are found to occur depending on coupling strength, with distinct signatures in physical properties. For strong interimpurity coupling, a residual chain spin- $\frac{1}{2}$ moment experiences a renormalized effective coupling to the leads, while in the weak-coupling regime, Kondo coupling is mediated via incipient single-channel Kondo singlet formation. We also investigate models in which the leads are tunnel-coupled to the impurity chain, permitting variable dot filling under applied gate voltages. Effective low-energy models for each regime of filling are derived, and for even fillings where the chain ground state is a spin singlet, an orbital 2CK effect is found to be operative. Provided mirror symmetry is preserved, 2CK physics is shown to be wholly robust to variable dot filling; in particular, the single-particle spectrum at the Fermi level, and hence the low-temperature zero-bias conductance, is always pinned to half-unity. We derive a Friedel-Luttinger sum rule and from it show that, in contrast to a Fermi liquid, the Luttinger integral is nonzero and determined solely by the “excess” dot charge as controlled by gate voltage. The relevance of the work to real quantum dot devices, where interlead charge-transfer processes fatal to 2CK physics are present, is also discussed. Physical arguments and numerical renormalization-group techniques are used to obtain a detailed understanding of these problems.

DOI: [10.1103/PhysRevB.84.035119](https://doi.org/10.1103/PhysRevB.84.035119)

PACS number(s): 71.27.+a, 72.15.Qm, 73.63.Kv, 71.10.Hf

I. INTRODUCTION

Non-Fermi-liquid (NFL) behavior is famously realized in the two-channel Kondo (2CK) model,¹ in which a single spin- $\frac{1}{2}$ impurity is exchange-coupled to two equivalent but independent metallic conduction bands. Its fascination for theorists is evident in the wide range of techniques applied to the model, including notably the Bethe ansatz,^{2–6} numerical renormalization group,^{6–10} and conformal field theory^{10–13} (for a review, see Ref. 14). Such methods have elucidated key aspects of the NFL state arising from “overscreening” of the impurity spin below the low-energy 2CK scale,¹ T_K^{2CK} , including exotic physical properties such as a residual entropy of $\frac{1}{2} \ln(2)$, and a logarithmically divergent low-temperature magnetic susceptibility, which are symptomatic of the frustration inherent when two conduction channels compete to screen the impurity local moment.¹⁴ NFL scaling of the conductance has also been predicted theoretically^{13–17} and measured experimentally¹⁸ in quantum dots, with its square-root temperature dependence being a characteristic signature of the 2CK phase.

This is all of course in marked contrast to standard Fermi liquid (FL) behavior,¹⁹ arising, for example, in the single-channel spin- $\frac{1}{2}$ Kondo or Anderson models¹⁹ (realized in practice in, e.g., ultrasmall quantum dots^{20,21}). Here, the dot spin is completely screened by a single bath of conduction electrons. The impurity entropy is in consequence quenched on the lowest energy scales, and the susceptibility is constant.¹⁹ Such systems are characterised by a unitarity zero-bias conductance, with a quadratic temperature dependence at low energies.²²

But the NFL physics of the 2CK model is delicate: finite channel asymmetry and/or interchannel charge transfer ultimately drive any real system out of the NFL regime^{11,14}

to a FL ground state. The exquisite tunability of quantum dot devices²³ allows for the manipulation of such perturbations; indeed, couplings can be fine-tuned via application of gate voltages to effectively eliminate channel asymmetry. However, tunnel coupling in such systems must result in some degree of charge transfer between the metallic “leads.” This is of course responsible for the predominance of *single-channel* Kondo physics in real quantum dot systems.

Suppressing interchannel charge transfer allows for the emergence of 2CK physics at intermediate temperatures and energies, although the instability of the 2CK fixed point to charge transfer means that an incipient NFL state forming at $T \sim T_K^{2CK}$ is subsequently destroyed below a FL crossover scale T_{FL} . Observation of NFL behavior at higher temperatures thus depends on a clear separation of scales, $T_{FL} \ll T_K^{2CK}$. This was achieved recently¹⁸ through use of an *interacting* lead tuned to the Coulomb blockade regime, and to date it is the only unambiguous experimental demonstration of the 2CK effect. Alternatively, sequential tunneling through several coupled dots should suppress charge transfer between leads,²⁴ and this could be exploited to access 2CK physics, although the interplay between spin and orbital degrees of freedom in coupled quantum dot systems can also generate new physics, as is well known both theoretically^{24–46} and experimentally.^{18,47–56}

In light of the above, we consider here odd-membered coupled quantum dot chains (each end of which is connected to its own metallic lead), and we demonstrate that 2CK physics is indeed generally accessible in these systems. In models in which the couplings are of pure exchange type, we show that the low-energy behavior is described by the channel-asymmetric two-channel Kondo model,¹⁴ with pristine 2CK physics surviving down to the lowest energy scales in the mirror-symmetric systems of most interest. Such models are

considered in Sec. II, where analytic predictions are confirmed and supplemented by use of Wilson's numerical renormalization group (NRG) technique⁵⁷⁻⁶¹ (for a recent review, see Ref. 59). In particular, universal scaling of thermodynamic and dynamic properties is demonstrated for odd chains of different length, and for systems with different coupling strengths. While the underlying 2CK physics of such systems is shown to be robust for finite antiferromagnetic exchange coupling, we find that the mechanism of overscreening differs according to whether the interimpurity coupling is strong or weak. In the former case (Sec. II A), it is the single lowest spin- $\frac{1}{2}$ state of the chain that effectively couples to and is overscreened by the leads, while for weak interimpurity coupling (Sec. II B), two-channel Kondo coupling is mediated via incipient *single-channel* Kondo singlets. Clear signatures of the latter are evident in the behavior of the frequency-dependent t matrix, the results for which are presented and analyzed.

To investigate conductance across two-channel coupled quantum dot chains, we study in Sec. III a related class of models in which the terminal impurities are Anderson-like quantum *levels*, tunnel-coupled to their respective metallic leads (although with interlead charge transfer still precluded by interimpurity exchange couplings). In the mirror-symmetric systems considered, we derive effective low-energy 2CK models valid for each regime of electron filling. Even-occupation filling regimes—where the chain ground state is a spin-singlet—are found in particular to exhibit an *orbital* 2CK effect, with spin playing the role of a channel index. As a consequence, 2CK physics is found to be robust throughout all regimes of electron-filling induced by changes in gate voltage.

Single-particle dynamics for such systems are then considered, and hence conductance (Sec. III C 1), the S matrix, and associated phase shifts (Sec. III D), again highlighting the universality arising at low energies. It is found in particular that the Fermi level value of the $T = 0$ single-particle spectrum—and hence the zero-bias conductance—is pinned to a half-unitary value, irrespective of electron-filling. A Friedel-Luttinger sum rule⁶² is then derived in Sec. III E, relating the Fermi level value of the spectrum to the “excess” charge due to the quantum dot chain and the Luttinger integral.^{63,64} By virtue of the spectral pinning, the sum rule relates directly the Luttinger integral to the excess charge/dot filling, in contrast to a Fermi liquid, where it is the Luttinger integral that is ubiquitously “pinned” (to zero),^{63,64} and the dot filling then determines the value of the spectrum at the Fermi level.^{19,65}

Finally, in Sec. IV we consider briefly the applicability of our findings to real coupled quantum dot devices. We argue that the effective low-energy model describing such systems is generically a 2CK model with both channel-asymmetry and interlead cotunneling charge transfer. Via a suitable basis transformation, one obtains a model in which charge transfer between even and odd channels is eliminated, from which the underlying behavior is readily understood in terms of that of a pure channel-asymmetric 2CK model. The t matrix (and hence spectrum) in a given physical channel is, however, related via this transformation to a combination of t matrices in even and odd channels, respectively. In the mirror-symmetric case sought experimentally, this leads to the striking conclusion that for sufficiently small but nonvanishing cotunneling charge transfer, the crossover *out* of the NFL regime is not in fact

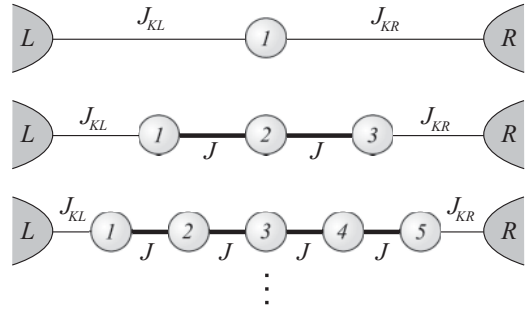


FIG. 1. Schematic illustration of odd-membered impurity chains, each end of which is coupled to its own metallic lead.

apparent in conductance measurements, despite the ultimate low-energy physics being that of a Fermi liquid.

II. 2CK HEISENBERG CHAINS

We consider a chain of N_c coupled spin- $\frac{1}{2}$ impurities, each end of which is also coupled to its own metallic lead, as illustrated in Fig. 1. To investigate 2CK physics, we study explicitly in this section a system of exchange-coupled spin- $\frac{1}{2}$ impurities, where interlead charge transfer is eliminated from the outset. For an impurity chain of length N_c , the full Hamiltonian is thus $H^{N_c} = H_L + H_c^{N_c} + H_R^{N_c}$. Here $H_L = \sum_{\alpha, \mathbf{k}, \sigma} \epsilon_{\mathbf{k}} a_{\alpha \mathbf{k} \sigma}^\dagger a_{\alpha \mathbf{k} \sigma}$ refers to the two equivalent noninteracting metallic leads ($\alpha = L/R$), and

$$H_c^{N_c} = J \sum_{i=1}^{N_c-1} \hat{\mathbf{S}}_i \cdot \hat{\mathbf{S}}_{i+1}, \quad (1a)$$

$$H_R^{N_c} = J_{KL} \hat{\mathbf{S}}_1 \cdot \hat{\mathbf{s}}_{L0} + J_{KR} \hat{\mathbf{S}}_{N_c} \cdot \hat{\mathbf{s}}_{R0}, \quad (1b)$$

where $\hat{\mathbf{S}}_i$ is a spin- $\frac{1}{2}$ operator for impurity i , and $\hat{\mathbf{s}}_{\alpha 0}$ is the spin density of lead $\alpha = L/R$ at impurity $1(N_c)$:

$$\hat{\mathbf{s}}_{\alpha 0} = \sum_{\sigma, \sigma'} f_{\alpha 0 \sigma}^\dagger \boldsymbol{\sigma}_{\sigma \sigma'} f_{\alpha 0 \sigma'}, \quad (2a)$$

$$f_{\alpha 0 \sigma}^\dagger = \frac{1}{\sqrt{N}} \sum_{\mathbf{k}} a_{\alpha \mathbf{k} \sigma}^\dagger, \quad (2b)$$

with $\boldsymbol{\sigma}$ the Pauli matrices and $f_{\alpha 0 \sigma}^\dagger$ the creation operator for the “0” orbital of the $\alpha = L/R$ Wilson chain ($N \rightarrow \infty$ is the number of orbitals or \mathbf{k} states in the chain).

In the following, we focus on odd- N_c chains, with antiferromagnetic (AF) exchange couplings for both the intrachain Heisenberg exchange, $J > 0$, and the Kondo exchanges, $J_{K\alpha} > 0$. (We do not consider here even- N_c chains, where the generic low-energy physics is quite different and in essence that of the two-impurity Kondo model.) We also consider both the channel symmetric case, $J_{KR} = J_{KL}$, as well as the more general case in which channel asymmetry is present, $J_{KR} \neq J_{KL}$. The simplest member of the family, $N_c = 1$, is of course the classic single-spin 2CK model,^{1,14} while variants of the $N_c = 3$ trimer have also been considered previously.³⁸⁻⁴⁵ We show below that an effective single-spin 2CK model results in all cases, from which universal 2CK physics is expected on the lowest energy scales in the channel-symmetric case,

although the mechanism by which the effective two-channel coupling arises is rather different in the strong and weak interimpurity coupling regimes.

A. Strong interimpurity coupling

We consider first the case in which the interimpurity exchange couplings J are sufficiently large that only the ground state of the isolated spin chain is relevant in constructing the effective low-energy model upon coupling to the leads. As detailed in Sec. II B, this means in practice $J \gtrsim T_{K,\alpha}^{\text{1CK}}$, with $T_{K,\alpha}^{\text{1CK}}$ the scale for single-channel Kondo quenching of a terminal spin to lead α , arising in the ‘‘uncoupled’’ $J = 0$ limit. The lowest state of an AF-coupled odd-membered spin- $\frac{1}{2}$ chain is of course a spin doublet, the components of which we label as $|N_c; S^z = \pm \frac{1}{2}\rangle$. All other states are at least $O(J/N_c)$ higher in energy.

1. Effective 2CK model

To leading order in $J_{K\alpha}$, the low-energy model is then obtained simply by projecting into the reduced Hilbert space of the lowest doublet for a chain of length N_c , using

$$\hat{1}_{N_c} = \sum_{S^z} |N_c; S^z\rangle \langle N_c; S^z|. \quad (3)$$

The resultant Hamiltonian $H_{\text{eff}}^{N_c} = \hat{1}_{N_c} H_c^{N_c} \hat{1}_{N_c}$ follows as

$$H_{\text{eff}}^{N_c} = \frac{1}{2} J_K \hat{1}_{N_c} (\hat{\mathbf{S}}_1 + \hat{\mathbf{S}}_{N_c}) \hat{1}_{N_c} \cdot (\hat{\mathbf{s}}_{L0} + \hat{\mathbf{s}}_{R0}) + \frac{1}{2} \delta_K \hat{1}_{N_c} (\hat{\mathbf{S}}_1 + \hat{\mathbf{S}}_{N_c}) \hat{1}_{N_c} \cdot (\hat{\mathbf{s}}_{L0} - \hat{\mathbf{s}}_{R0}), \quad (4)$$

where $J_K = \frac{1}{2}(J_{KL} + J_{KR})$ and $\delta_K = \frac{1}{2}(J_{KL} - J_{KR})$, and we use the symmetry $\hat{1}_{N_c} \hat{\mathbf{S}}_1 \hat{1}_{N_c} = \hat{1}_{N_c} \hat{\mathbf{S}}_{N_c} \hat{1}_{N_c}$.

In the absence of a magnetic field, \uparrow/\downarrow spin symmetry implies $\hat{P}_{\uparrow\downarrow} |N_c; S^z\rangle = \gamma |N_c; -S^z\rangle$, where $\hat{P}_{\uparrow\downarrow}$ permutes simultaneously all up and down spins, and $\gamma = \pm 1$ only since $\hat{P}_{\uparrow\downarrow}^2 = \hat{1}$.⁴⁵ Together with $\hat{P}_{\uparrow\downarrow} \hat{S}_i^z = -\hat{S}_i^z \hat{P}_{\uparrow\downarrow}$, it follows directly that

$$\begin{aligned} & \langle N_c; S^z | \hat{S}_1^z + \hat{S}_{N_c}^z | N_c; S^z \rangle \\ &= -\langle N_c; -S^z | \hat{S}_1^z + \hat{S}_{N_c}^z | N_c; -S^z \rangle \propto S^z \end{aligned} \quad (5)$$

(as $|N_c; S^z\rangle$ is a spin doublet). Such matrix elements appear in the z component of the contraction in Eq. (4), and by spin isotropy an effective model of 2CK form results:

$$H_{\text{eff}}^{N_c} = J_{K,N_c}^{\text{eff}} \hat{\mathbf{S}} \cdot (\hat{\mathbf{s}}_{L0} + \hat{\mathbf{s}}_{R0}) + \delta_{K,N_c}^{\text{eff}} \hat{\mathbf{S}} \cdot (\hat{\mathbf{s}}_{L0} - \hat{\mathbf{s}}_{R0}), \quad (6)$$

where $\hat{\mathbf{S}}$ is a spin- $\frac{1}{2}$ operator for the lowest chain doublet, defined by $\hat{S}^z = \sum_{S^z} |N_c; S^z\rangle S^z \langle N_c; S^z|$ and $\hat{S}^{\pm} = |N_c; \pm \frac{1}{2}\rangle \langle N_c; \mp \frac{1}{2}|$. The effective couplings are given by

$$J_{K,N_c}^{\text{eff}} = \langle N_c; +\frac{1}{2} | \hat{S}_1^z + \hat{S}_{N_c}^z | N_c; +\frac{1}{2} \rangle J_K, \quad (7a)$$

$$\delta_{K,N_c}^{\text{eff}} = \langle N_c; +\frac{1}{2} | \hat{S}_1^z + \hat{S}_{N_c}^z | N_c; +\frac{1}{2} \rangle \delta_K. \quad (7b)$$

Numerical evaluation of Eq. (7) for odd N_c yields an AF effective coupling, $J_{K,N_c}^{\text{eff}} > 0$, which is renormalized with respect to the bare coupling and diminishes as the chain length increases, as shown in Table I.

Hence, for sufficiently low temperatures $T \ll J/N_c$, the low-energy behavior of the system is equivalent to the single-spin 2CK model.¹⁴ In the L/R mirror-symmetric case, $J_{KL} =$

TABLE I. Effective couplings.

N_c	$J_{K,N_c}^{\text{eff}}/J_K$
1	1
3	$\frac{2}{3}$
5	0.51...
7	0.42...

J_{KR} ($\delta_K = \delta_K^{\text{eff}} = 0$), the stable $T = 0$ fixed point (FP) is then the infrared 2CK FP. The lowest spin- $\frac{1}{2}$ state of the impurity chain is thus overscreened by conduction electrons, giving rise to a residual entropy of $S_{\text{imp}} = \frac{1}{2} \ln(2)$ ($k_B = 1$), a hallmark of the NFL 2CK ground state.¹⁴ Overscreening sets in below a characteristic scale T_K^{2CK} , given from perturbative scaling¹ as

$$T_K^{\text{2CK}} \sim J_{K,N_c}^{\text{eff}} \exp(-1/\rho J_{K,N_c}^{\text{eff}}), \quad (8)$$

where $\rho = 1/(2D)$ is the lead density of states per orbital (assumed to be uniform) and $2D$ is the bandwidth.

By contrast, when strict L/R mirror symmetry is broken via distinct exchange couplings to the two leads, $J_{KL} \neq J_{KR}$ (i.e., $\delta_K \neq 0$), the 2CK FP is destabilized in the full model Eq. (1). This behavior is of course well known from the single-spin 2CK model with channel anisotropy,^{1-3,10,14} where the impurity local moment is fully screened by conduction electrons in the more strongly coupled lead, and a Fermi liquid ground state results. For $\delta_K > 0$, under renormalization on reduction of the temperature or energy scale, the system flows to *strong coupling* (SC) with the left lead ($J_{KL} \rightarrow \infty$) while the right lead decouples ($J_{KR} \rightarrow 0$).^{1-3,10,14} The stable $T = 0$ FP thus depends on the *sign* of δ_K , with ‘‘SC:L’’ describing the lowest energy behavior for $\delta_K > 0$ while ‘‘SC:R’’ is stable for $\delta_K < 0$. The mirror-symmetric case, $\delta_K = 0$, is as such the quantum critical point separating phases where a Kondo singlet forms in either the L or R lead.

In the full model, effective *single-channel* Kondo screening characteristic of flow to the Fermi liquid FP in channel-asymmetric systems sets in below a characteristic scale, which can likewise be obtained from perturbative scaling:¹

$$T_K^{\text{SC}} \sim J_{K,N_c}^{\text{SC}} \exp(-1/\rho J_{K,N_c}^{\text{SC}}), \quad (9)$$

where $J_{K,N_c}^{\text{SC}} = J_{K,N_c}^{\text{eff}} + |\delta_{K,N_c}^{\text{eff}}|$ is the effective coupling between the lowest chain doublet state and the more strongly coupled lead.

2. NRG results: Symmetric case

The above picture indicates that in the mirror-symmetric case, $\delta_K = 0$, the lowest energy behavior for all odd chains should be that of the single-spin 2CK model,¹⁴ but with renormalized effective couplings [Eq. (7) and Table I] and hence from Eq. (8) a reduced 2CK scale, T_K^{2CK} .

We now analyze the full model, Eq. (1), for odd $N_c = 1, 3, 5, 7$ using Wilson’s NRG technique,⁵⁷⁻⁵⁹ employing a complete basis set of the Wilson chain⁶⁰ to calculate the full density matrix.^{60,61} Calculations here are typically performed using an NRG discretization parameter $\Lambda = 3$, retaining the lowest $N_s = 4000$ states per iteration. We consider first the impurity contribution^{58,59} to thermodynamics $\langle \hat{\Omega} \rangle_{\text{imp}} =$

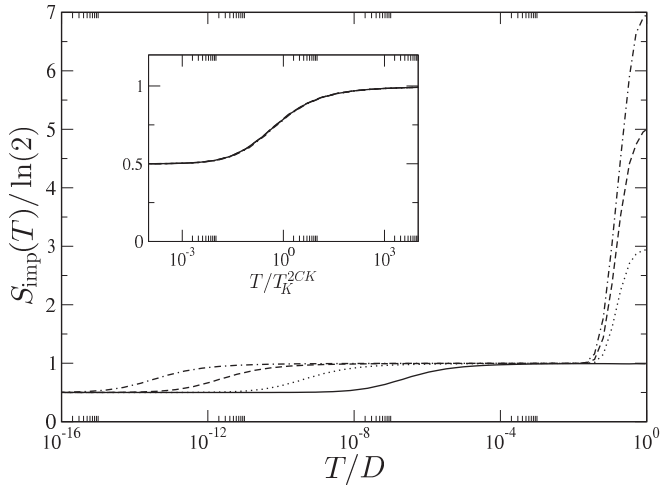


FIG. 2. Entropy $S_{\text{imp}}(T)/\ln(2)$ vs T/D for chains of length $N_c = 1, 3, 5, 7$ (solid, dotted, dashed, and dot-dashed lines, respectively) in the large interimpurity coupling regime. Shown for $\rho J = 0.15$ and $\rho J_K = 0.075$ in the L/R -symmetric limit $\delta_K = 0$. Inset: scaling collapse onto the universal 2CK curve.

$\langle \hat{\Omega} \rangle - \langle \hat{\Omega} \rangle_0$, with $\langle \hat{\Omega} \rangle_0$ denoting a thermal average in the absence of the impurity chain. We focus in particular on the entropy, $S_{\text{imp}}(T)$, and the uniform spin susceptibility, $\chi_{\text{imp}}(T) = \langle (\hat{S}^z)^2 \rangle_{\text{imp}}/T$ (here \hat{S}^z refers to the spin of the entire system), the temperature dependences of which provide clear signatures of the underlying FP's reached under renormalization on progressive reduction of the temperature or energy scale.^{58,59}

Figure 2 shows representative NRG results for the T dependence of the entropy, for odd chains with $N_c = 1, 3, 5, 7$. At high temperatures, the impurities are effectively uncoupled, so the chain contribution to the entropy is $S_{\text{imp}} = N_c \ln(2)$, as is seen clearly from Fig. 2. On the scale of $T \sim J/N_c$, all but the lowest chain doublet are projected out, the entropy then dropping as expected to $\ln(2)$ in all cases. Renormalization-group (RG) flow to this local moment (LM) FP^{1,58} marks the regime of validity of the effective single-spin 2CK model, Eq. (6). The local moment is then overscreened^{1,14} by symmetric coupling to the two leads on an exponentially small scale, $T_K^{2\text{CK}}$, the $T = 0$ residual entropy in all cases being $\frac{1}{2} \ln(2)$. $T_K^{2\text{CK}}$ itself is determined in practice from $S_{\text{imp}}(T_K^{2\text{CK}}) = \frac{3}{4} \ln(2)$ (suitably between the characteristic LM and 2CK FP values). The exponential reduction of the 2CK scale with increasing chain length (evident in Fig. 2) is expected from Eq. (8), which depends on N_c through the effective coupling given in Table I. The inset shows the data rescaled in terms of $T/T_K^{2\text{CK}}$. The low-temperature behavior of all odd chains collapses to the universal scaling curve for the single-spin 2CK model (i.e., the $N_c = 1$ case, solid line), likewise known from, e.g., the Bethe ansatz solution,²⁻⁶ confirming the mapping of the full model to Eq. (6).

The above FP structure and energy scales also naturally show up in the magnetic susceptibility, as seen in Fig. 3. At the highest temperatures, $T\chi_{\text{imp}} = \frac{1}{4}N_c$, as expected^{19,58} for N_c free spins. Flow to the LM FP on the scale $T \sim J/N_c$ is again clearly evident in the drop to $T\chi_{\text{imp}} = \frac{1}{4}$, corresponding

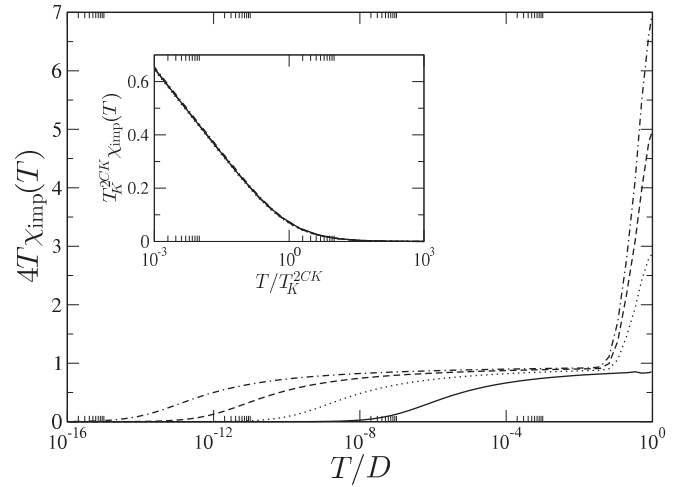


FIG. 3. Spin susceptibility $4T\chi_{\text{imp}}(T)$ vs T/D for the same parameters as Fig. 2: scaling collapse of $\chi_{\text{imp}}(T)$ itself onto the universal 2CK curve, with characteristic NFL form $T_K^{2\text{CK}}\chi_{\text{imp}}(T) = \alpha \ln(T_K^{2\text{CK}}/T)$.

to the expected Curie law behavior. On the scale $\sim T_K^{2\text{CK}}$, the susceptibility drops to $T\chi_{\text{imp}} = 0$, which remains its $T = 0$ value. The inset shows $T_K^{2\text{CK}}\chi_{\text{imp}}(T)$ vs $T/T_K^{2\text{CK}}$, showing scaling collapse to the universal single-spin 2CK curve, and demonstrating the characteristic NFL logarithmic divergence¹⁴ of the susceptibility χ_{imp} itself on approaching the 2CK FP.

We turn now to dynamics, in particular the low-energy Kondo resonance embodied in the spectrum $D\rho_K(\omega) \equiv D\rho_{K,\alpha}(\omega) = -\pi\rho_T \text{Im}[t_\alpha(\omega)]$, where $t_\alpha(\omega) \equiv t(\omega)$ is the t matrix¹⁹ for the $\alpha = L/R$ lead (equivalent by symmetry for $\delta_K = 0$), and $\rho_T = N\rho$ is the total lead density of states. Using equation of motion techniques^{19,66} yields

$$\pi\rho_T t_\alpha(\omega) = \frac{\pi}{4} \rho J_{K\alpha}^2 \tilde{G}_{\alpha i}(\omega) \quad (10)$$

with $i = 1$ for $\alpha = L$ and $i = N_c$ for $\alpha = R$, where

$$\tilde{G}_{\alpha i}(\omega) = \langle \langle \hat{S}_i^- f_{\alpha 0\downarrow} + \hat{S}_i^z f_{\alpha 0\uparrow} + \hat{S}_i^+ f_{\alpha 0\downarrow} + \hat{S}_i^z f_{\alpha 0\uparrow} \rangle \rangle_\omega \quad (11)$$

and $\langle \langle \hat{A}; \hat{B} \rangle \rangle_\omega$ is the Fourier transform of the retarded correlator $\langle \langle \hat{A}(t_1); \hat{B}(t_2) \rangle \rangle = -i\theta(t_1 - t_2) \langle \langle \hat{A}(t_1), \hat{B}(t_2) \rangle \rangle$. The correlator in Eq. (11) can be calculated directly within NRG,⁵⁹⁻⁶¹ hence enabling access to the spectrum $D\rho_K(\omega)$. However, an alternative expression for the t matrix can be obtained in the spirit of Ref. 67, and in the wide flat-band case considered here it is simply

$$\pi\rho_T t_\alpha(\omega) = -i \left[1 + \left(\frac{2}{\pi\rho J_{K\alpha}} \right)^2 \frac{G_{\alpha 0}(\omega)}{\tilde{G}_{\alpha i}(\omega)} \right]^{-1} \quad (12)$$

where $G_{\alpha 0}(\omega) = \langle \langle f_{\alpha 0\sigma}; f_{\alpha 0\sigma}^\dagger \rangle \rangle_\omega$ is the Green function for the “0” orbital of the $\alpha = L/R$ Wilson chain.⁵⁷ The quotient of correlators in Eq. (12) is found to improve greatly numerical accuracy, and is employed in the following.

Figure 4 shows the resultant spectrum $D\rho_K(\omega)$ vs ω/D for chains of length $N_c = 1, 3, 5, 7$ with the same parameters as Figs. 2 and 3 [noting that $\rho_K(\omega) = \rho_K(-\omega)$ since the model, Eq. (1), is particle-hole symmetric]. The low-energy form of each spectrum naturally reflects RG flow in the

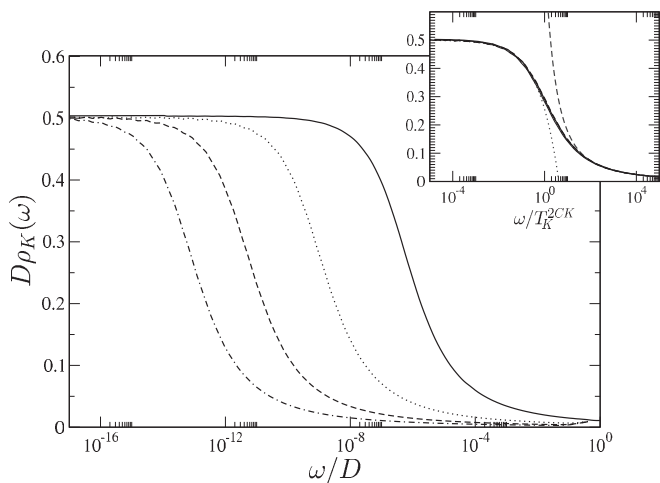


FIG. 4. $T = 0$ spectrum $D\rho_K(\omega)$ vs ω/D for the same parameters as Fig. 2. Inset: vs $\omega/T_K^{2\text{CK}}$, showing collapse to the scaling spectrum for odd chains. Gray dotted line: low- $|\omega|/T_K^{2\text{CK}} \ll 1$ asymptotic behavior $D\rho_K(\omega) = \frac{1}{2}[1 - b(|\omega|/T_K^{2\text{CK}})^{1/2}]$; gray dashed line: high- $|\omega|/T_K^{2\text{CK}} \gg 1$ scaling behavior, $D\rho_K(\omega) = A/[\ln^2(|\omega|/T_K^{2\text{CK}}) + B]$.

vicinity of the 2CK FP, as studied also in a variety of different models that exhibit 2CK behavior.^{13,42,45,68–71} In particular, for all odd chains, a half-unitarity value is seen to arise at the Fermi level, $D\rho_K(\omega = 0) = \frac{1}{2}$, and collapse to the universal single-spin 2CK scaling spectrum is clearly evident in the inset to Fig. 4. The leading low-frequency asymptotic behavior is $D\rho_K(\omega) = \frac{1}{2}[1 - b(|\omega|/T_K^{2\text{CK}})^{1/2}]$ (in marked contrast to the form $[1 - a(|\omega|/T_K)^2]$ characteristic¹⁹ of RG flow near a Fermi liquid FP), and with which the numerics agree well for $\omega \ll T_K^{2\text{CK}}$. At high frequencies $\omega \gg T_K^{2\text{CK}}$, in contrast, the leading asymptotic behavior of the scaling spectrum is $D\rho_K(\omega) = A/[\ln^2(|\omega|/T_K^{2\text{CK}}) + B]$, which behavior is common to other models in which spin-flip scattering processes are important at high energies,⁷² such as the single-channel Anderson or Kondo models.

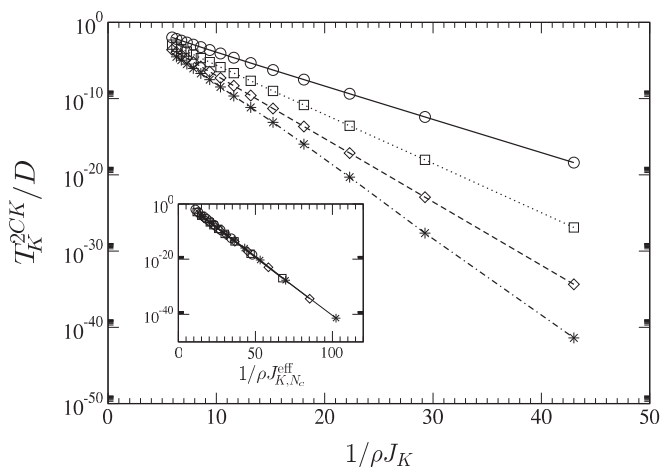


FIG. 5. Kondo temperature $T_K^{2\text{CK}}/D$ vs $1/\rho J_K$ for chains of length $N_c = 1, 3, 5, 7$ (circles, squares, diamonds, and stars, respectively, with lines as a guide to the eye) and common exchange coupling $\rho J = 0.15$. Inset: scaling collapse to common linear form when plotted vs $1/\rho J_{K,N_c}^{\text{eff}}$ [given by Eq. (7)].

Finally, we consider the evolution of the 2CK scale itself as the impurity-lead coupling is varied in the mirror-symmetric case, shown vs $1/\rho J_K$ in Fig. 5 for chains of length $N_c = 1, 3, 5, 7$. An exponential dependence of the 2CK scale on the impurity-lead coupling is expected from Eq. (8), and seen clearly in the main panel. The differing slopes reflect the renormalization of the bare Kondo coupling $J_K \rightarrow J_{K,N_c}^{\text{eff}}$ with increasing impurity chain length (Table I), collapse to common linear behavior being observed in the inset where the 2CK scales are plotted vs $1/\rho J_{K,N_c}^{\text{eff}}$, establishing thereby quantitative agreement with Eqs. (7) and (8) and Table I, and hence the mapping to the effective 2CK model, Eq. (6).

3. NRG results: Asymmetric case

We turn now to the channel-asymmetric case, $J_{KL} \neq J_{KR}$ (i.e., $\delta_K \neq 0$). The effective model Eq. (6) should describe the low-energy behavior of all odd chains, so the rich physics of the *asymmetric* single-spin 2CK model^{1–3,10,14} is thus expected for $T \ll J/N_c$. As discussed above, breaking L/R mirror symmetry is a relevant perturbation¹⁰ to the 2CK FP, so FL physics will arise generically on the lowest energy scales. Indeed, in the limit of maximal asymmetry $J_K = \delta_K$, the right lead is completely decoupled in Eq. (6); pristine single-channel Kondo (1CK) screening by the left lead then results below a single-channel scale $T_K^{1\text{CK}}$. For $\delta_K \ll T_K^{1\text{CK}}$, however, RG flow in the vicinity of the 2CK FP strongly affects the behavior at higher temperatures and energies.^{1–3,10,14} This is indeed seen in Fig. 6(a), where the entropy $S_{\text{imp}}(T)$ vs T/D is shown for a representative system with $N_c = 3$, $\rho J = 0.25$, and $\rho J_K = 0.125$, varying $\rho \delta_K = 10^{-1}, 10^{-2}, 10^{-3}, 10^{-4}, 10^{-5}, 10^{-6}$, and 10^{-7} [lines (a)–(g)], successively approaching the quantum critical point at the symmetric limit, $\delta_K = 0$: line (h). The scale $T_K^{1\text{CK}}$ (for which $\rho J_K = \rho \delta_K$) is $\rho T_K^{1\text{CK}} \approx 10^{-3}$ here, and sets the scale for the crossover from “large” to “small” channel asymmetry ($\rho \delta_K \gg \rho T_K^{1\text{CK}}$ and $\ll \rho T_K^{1\text{CK}}$, respectively).

At the highest temperatures, the three impurity spins are effectively free, yielding trivially a common entropy $S_{\text{imp}} = 3 \ln(2)$. As T is lowered, all but the lowest trimer doublet state is projected out, heralding flow to the LM FP, with characteristic^{1,58} entropy $S_{\text{imp}} = \ln(2)$. For large channel asymmetry [e.g., lines (a) and (b)], RG flow is then directly to the SC:L FP: the impurity spin is fully screened^{1–3,10,14} by the formation of a Kondo singlet with conduction electrons in the left lead ($\delta_K > 0$) below an effective single-channel Kondo scale T_K^{SC} , and hence $S_{\text{imp}} = 0$ for $T \ll T_K^{\text{SC}}$. The Kondo scale itself is given by Eq. (9) in the large δ_K regime,⁷⁴ with an effective Kondo coupling $J_{K,N_c=3}^{\text{eff}} = \frac{2}{3}(J_K + |\delta_K|)$ for $N_c = 3$ (see Table I).

In the case of smaller channel asymmetry, $\rho \delta_K \ll \rho T_K^{1\text{CK}}$, RG flow to the stable Fermi liquid SC:L FP occurs via the critical FP, which is of course the 2CK FP. The chain spin- $\frac{1}{2}$ associated with the LM FP is then fully screened in a *two-stage* process [Fig. 6(a)]. All such systems flow first to the 2CK FP on a common scale $T_K^{2\text{CK}}$, given by Eq. (8). The entropy thus drops to $S_{\text{imp}} = \frac{1}{2} \ln(2)$, symptomatic¹⁴ of overscreening, before being quenched completely below a scale $T \sim T^*$ characterizing^{1–3,10,14} the flow to the SC:L FP [with T^* defined in practice by $S_{\text{imp}}(T^*) = \frac{1}{4} \ln 2$]. A clear

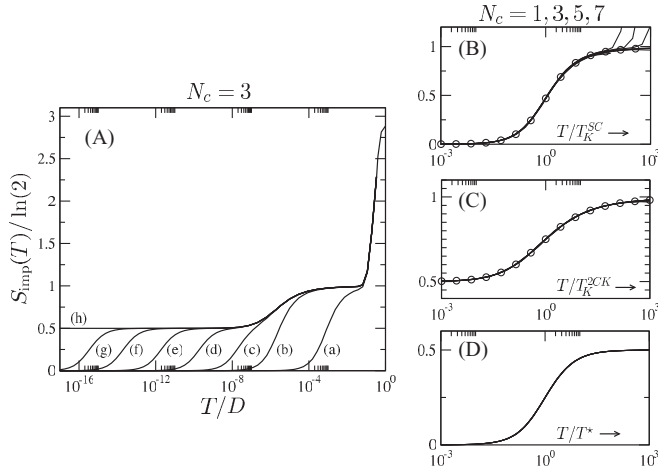


FIG. 6. (A) Entropy $S_{\text{imp}}(T)/\ln(2)$ vs T/D on progressively approaching the transition, for $N_c = 3$. Shown for fixed $\rho J = 0.25$ and $\rho J_K = 0.125$, varying $\rho\delta_K = 10^{-1}, 10^{-2}, 10^{-3}, 10^{-4}, 10^{-5}, 10^{-6}$, and 10^{-7} [lines (a)–(g)], with the symmetric point $\rho\delta_K = 0$ shown as line (h). (B) Scaling collapse to the 1CK curve (circles) for strong channel asymmetry, $\rho\delta_K = 10^{-1}$ and 10^{-2} , with $N_c = 1, 3, 5, 7$. (C) For small asymmetry ($\rho\delta_K = 10^{-6}$ and 10^{-7}), and $N_c = 1, 3, 5, 7$. Showing universality in the LM \rightarrow 2CK FP crossover, on rescaling in terms of $T/T_K^{2\text{CK}}$, compared directly to the symmetric 2CK scaling curve (circles). (D) Same data as (C), now rescaled in terms of T/T^* , showing universal crossover from the 2CK FP ($S_{\text{imp}}/\ln 2 = \frac{1}{2}$) to the stable SC:L FP ($S_{\text{imp}} = 0$).

$S_{\text{imp}} = \frac{1}{2} \ln(2)$ plateau is thus seen for lines (d)–(g) in Fig. 6(a), with T^* diminishing rapidly as the transition is approached. The evolution of T^* on varying δ_K for different odd chains is itself studied in Fig. 8 below, and the result in the small- $|\delta_K|$ regime is a characteristic power-law decay,

$$T^* \delta_K \xrightarrow{0^\pm} \mathcal{A} |\delta_K|^\nu, \quad \nu = 2 \quad (13)$$

with exponent $\nu = 2$ and common amplitudes \mathcal{A} on approaching the transition at $\delta_K = 0$ from either side (as guaranteed by symmetry). Equation (13) generalizes the known result^{2,3,14} for the channel-anisotropic single-spin 2CK model, and is expected from the mapping of the full chain model [Eq. (1)] onto the effective model, Eq. (6).

We now turn to the scaling behavior of the entropy for chains of different length, as demonstrated by the three universal curves given in panels (B)–(D) of Fig. 6. First, in Fig. 6(B) for $N_c = 1, 3, 5, 7$, we show strongly asymmetric systems ($\rho\delta_K \gg \rho T_K^{1\text{CK}}$) with $\rho\delta_K = 10^{-1}$ and 10^{-2} . The data clearly collapse to common scaling form when scaled in terms of T/T_K^{SC} , indicative of universal one-stage quenching from the LM to the SC:L FP. Results for the single-channel spin- $\frac{1}{2}$ Kondo model are also shown (circles), confirming that the crossover is characterized by effective *single-channel* Kondo screening.

The situation is more subtle for weakly asymmetric systems $\rho\delta_K \ll \rho T_K^{1\text{CK}}$, where two-stage quenching occurs from the LM FP, through the 2CK FP, to the fully quenched SC:L FP. As now shown, *each* of these stages separately exhibit universal scaling, in terms of the two distinct low-energy scales $T_K^{2\text{CK}}$ and T^* , respectively. In Figs. 6(C) and 6(D) for $N_c = 1, 3, 5, 7$, systems close to the transition are shown. To determine the full

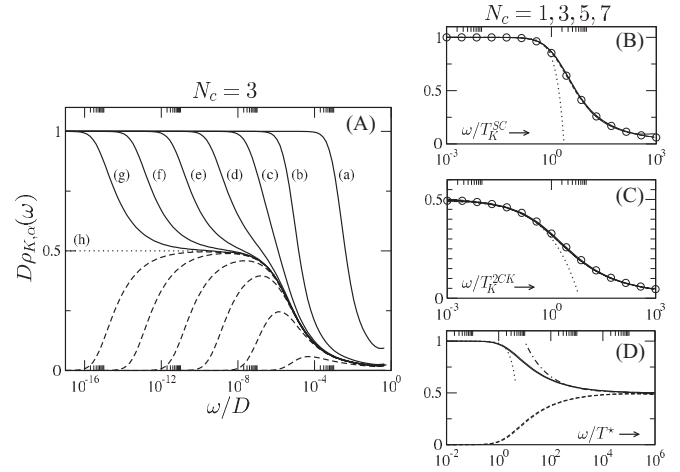


FIG. 7. (A) Spectra $D\rho_{K,\alpha}(\omega)$ (solid lines) and $D\rho_{K,R}(\omega)$ (dashed) vs ω/D on progressively approaching the transition for $N_c = 3$, using the same parameters as in Fig. 6. (B) Collapse of $D\rho_{K,L}(\omega)$ to the 1CK scaling spectrum (circles) in the strongly asymmetric limit, $\rho\delta_K = 10^{-1}$ and 10^{-2} , for $N_c = 1, 3, 5, 7$. The dotted line shows the asymptotic low- $|\omega|/T_K^{\text{SC}}$ FL behavior $D\rho_{K,L}(\omega) = 1 - a(|\omega|/T_K^{\text{SC}})^2$. (C) For small asymmetry ($\rho\delta_K = 10^{-6}$ and 10^{-7} for $N_c = 1, 3, 5, 7$), universal behavior arising on rescaling $D\rho_{K,\alpha}(\omega)$ for both $\alpha = L/R$ in terms of $\omega/T_K^{2\text{CK}}$, as compared with the symmetric 2CK scaling curve (circles). The dotted line shows the asymptotic ($T^* \ll |\omega| \ll T_K^{2\text{CK}}$) NFL behavior $D\rho_{K,\alpha}(\omega) = \frac{1}{2} [1 - b(|\omega|/T_K^{2\text{CK}})^{1/2}]$. (D) Same data rescaled in terms of T/T^* , showing the universal low-temperature crossover for $D\rho_{K,L}(\omega)$ (solid lines) and $D\rho_{K,R}(\omega) \equiv 1 - D\rho_{K,L}(\omega)$ (dashed). The $T^* \ll |\omega| \ll T_K^{2\text{CK}}$ asymptotic behavior $D\rho_{K,L}(\omega) = \frac{1}{2} [1 + c(|\omega|/T^*)^{-1/2}]$ is shown as a dot-dashed line, while for $|\omega| \ll T^*$, FL behavior results, $D\rho_{K,L}(\omega) = 1 - d(|\omega|/T^*)^2$ (dotted line).

universal curves, it is of course essential to obtain good scale separation of $T_K^{2\text{CK}}$ and T^* : here, $T_K^{2\text{CK}}/T^* > 10^8$.

In Fig. 6(C), results are rescaled in terms of $T/T_K^{2\text{CK}}$. Collapse to the universal scaling curve for the symmetric single-spin 2CK model (shown separately, circles) is seen clearly, the crossover from the LM FP ($S_{\text{imp}} = \ln 2$) to the 2CK FP ($S_{\text{imp}} = \frac{1}{2} \ln 2$) being as such determined by the 2CK scale $T_K^{2\text{CK}}$. By contrast, the universality of the crossover from the unstable 2CK FP to the stable low- T SC:L FP with $S_{\text{imp}} = 0$ is shown in Fig. 6(D). Here, on rescaling in terms of T/T^* , the data collapse to a universal form controlled by the low-energy scale T^* , itself vanishing [Eq. (13)] as the quantum critical point $\delta_K = 0$ is approached.

The FP structure and energy scales naturally show up also in dynamical quantities, such as the scattering t matrix, and hence the spectra $D\rho_{K,\alpha}(\omega)$. These are considered in Fig. 7. In panel (A), again for $N_c = 3$, we focus on $D\rho_{K,L}(\omega)$ (solid lines) and $D\rho_{K,R}(\omega)$ (dashed) for systems with the same parameters as Fig. 6(A). Results for $\delta_K < 0$ are not shown, the $\alpha = L$ and R spectra simply being exchanged under the transformation $\delta_K \leftrightarrow -\delta_K$.

$N_c = 3$ chains with $\rho\delta_K = 10^{-1}$ and 10^{-2} [strong channel-asymmetry, lines (a) and (b)] show a characteristic resonance in the left-channel spectrum, $D\rho_{K,L}(\omega)$, on the scale $|\omega| \sim T_K^{\text{SC}}$, with the Fermi level value in particular being $D\rho_{K,L}(0) = 1$. This is the single-channel Kondo resonance, as is physically natural for these strongly channel-asymmetric cases because

effective single-channel Kondo screening is operative,¹⁰ with the behavior thus expected to be that of the single-channel Kondo or Anderson models.¹⁹ In the particle-hole symmetric limit of the latter, the Friedel sum rule⁶⁵ guarantees satisfaction of the unitarity limit [$D\rho_{K,L}(0) = 1$], and in the scaling regime $|\omega| \ll J/N_c$, one expects the entire one-channel scaling spectrum to be recovered. This is considered in panel (B), where results for $N_c = 1, 3, 5, 7$ and $\rho\delta_K = 10^{-1}$ and 10^{-2} are shown, rescaled in terms of ω/T_K^{SC} : essentially perfect agreement is seen with the universal scaling spectrum for the single-channel Kondo model (shown separately as circles). For $T_K^{\text{SC}} \ll |\omega| \ll J/N_c$, the characteristic $D\rho_{K,L}(\omega) \sim A/[\ln^2(|\omega|/T_K^{\text{SC}}) + B]$ behavior typical of “high” energy spin-flip scattering⁷² arises, while for $|\omega| \ll T_K^{\text{SC}}$, canonical Fermi liquid behavior,¹⁹ $D\rho_{K,L}(\omega) = 1 - a(|\omega|/T_K^{\text{SC}})^2$, occurs as expected.

Spectra for the right lead and channel, $D\rho_{K,R}(\omega)$ [dashed lines (a) and (b) of panel (A)], are similarly described by the leading $\sim 1/\ln^2(|\omega|/T_K^{\text{SC}})$ logarithms at high energies. However, the upward renormalization of the effective Kondo coupling to the right lead—and hence RG flow toward the SC:R FP—is cut off at $|\omega| \sim T_K^{\text{SC}}$, below which frequency the impurity chain local moment becomes fully screened by strong coupling to the *left* lead. Thus $D\rho_{K,R}(\omega) = 0$ for $|\omega| \ll T_K^{\text{SC}}$, as observed directly from the NRG results in panel (A).

We now turn to lines (e)–(g) of Fig. 7(A) for $N_c = 3$ systems with much smaller channel asymmetry, $\rho\delta_K \ll \rho T_K^{\text{1CK}}$. For both $\alpha = L$ and R , a clear half-unitary plateau of $D\rho_{K,\alpha}(\omega) \simeq \frac{1}{2}$ arises for $T^* \ll |\omega| \ll T_K^{\text{2CK}}$, indicative of RG flow near the 2CK FP. For $|\omega| \sim T^*$, however, flow to the Fermi liquid SC:L FP occurs, such that $D\rho_{K,L}(\omega = 0) = 1$ and $D\rho_{K,R}(\omega = 0) = 0$ are again satisfied. As was seen from the entropy (Fig. 6), there are two universal scales in this regime associated with the crossover from the LM FP to the 2CK FP [see panel (C)] and from the 2CK FP to the SC:L FP [panel (D)].

In panel (C) of Fig. 7, results are shown for systems of chain length $N_c = 1, 3, 5, 7$ and small channel asymmetry, $\rho\delta_K = 10^{-6}$ and 10^{-7} . Each is rescaled in terms of ω/T_K^{2CK} , and collapse to the universal *symmetric* 2CK curve (circles) is seen in all cases—for *both* $\alpha = L$ and R spectra. In particular, for $|\omega| \ll T_K^{\text{2CK}}$ the characteristic NFL behavior is obtained, $D\rho_{K,\alpha}(\omega) = \frac{1}{2}[1 - b(|\omega|/T_K^{\text{2CK}})^{1/2}]$ (dotted line).

Finally, panel (D) shows the same data, but rescaled now in terms of $|\omega|/T^*$. Two universal spectra emerge: one for $D\rho_{K,L}(\omega)$ and one for $D\rho_{K,R}(\omega)$. The two scaling spectra are, however, found to be related simply by $D\rho_{K,R}(\omega) = 1 - D\rho_{K,L}(\omega)$, so we need consider only $D\rho_{K,L}(\omega)$ (solid line). For $\omega \gg T^*$, the relevant L/R symmetry-breaking operator dominates,¹⁰ driving RG flow away from the 2CK FP. Since the scaling dimension of this operator¹⁰ is $\frac{1}{2}$, one expects $D\rho_{K,L}(\omega) = \frac{1}{2}[1 + c(|\omega|/T^*)^{-1/2}]$ (as indeed found, dot-dashed line). By contrast, for $|\omega| \ll T^*$, irrelevant operators^{10,58} affect the RG flow in the vicinity of the stable FL FP, so one expects the leading low- $|\omega|/T^*$ asymptotics to be $D\rho_{K,L}(\omega) = 1 - d(|\omega|/T^*)^2$ (dotted line). Good agreement with the numerics is seen in both regimes and for both $\alpha = L/R$ spectra in Fig. 7(D).

As the critical point is approached [$|\delta_K| \rightarrow 0$; lines (a)→(h) in Fig. 7], the spectra fold progressively onto the 2CK spectrum itself [line (h)] down to lower and lower frequencies. The scale

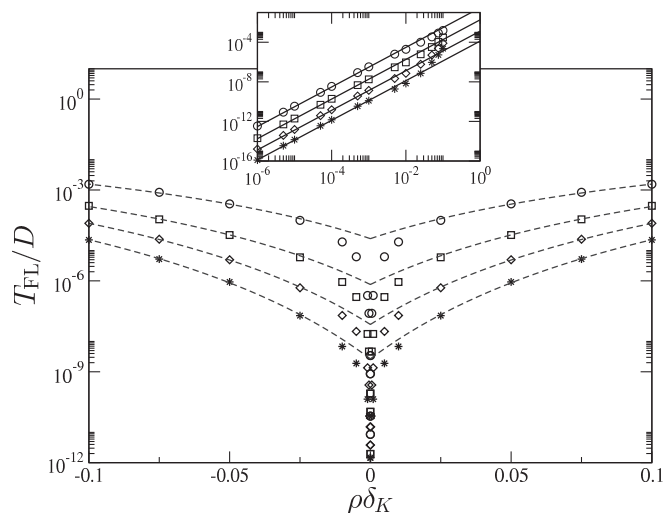


FIG. 8. Fermi liquid crossover temperature T_{FL}/D vs $\rho\delta_K$ for chains of length $N_c = 1, 3, 5, 7$ (circles, squares, diamonds, and stars) and couplings $\rho J = 0.25$ and $\rho J_K = 0.125$. For large channel asymmetry, $T_{\text{FL}} \equiv T_K^{\text{SC}}$: good agreement between the data and Eq. (9) (dashed lines) is seen for each N_c in the regime $|\rho\delta_K| \gtrsim 0.025$. The inset shows the small asymmetry behavior on a log-log plot. Here $T_{\text{FL}} \equiv T^*$, and the quadratic behavior of Eq. (13) is shown as the solid lines, onto which data fall cleanly for $|\rho\delta_K| \lesssim 0.01$.

T^* describing flow away from the 2CK FP vanishes according to Eq. (13), as is evident from the dynamics shown in Fig. 7 (or the thermodynamics in Fig. 6). In Fig. 8, the evolution of the low-energy scale as a function of channel asymmetry, $\rho\delta_K$, is examined. Since T_K^{SC} is the lowest energy scale of the problem in the large- $|\delta_K|$ regime, while T^* is the lowest scale for small $|\delta_K|$, we consider the generic crossover scale T_{FL} in Fig. 8, defined in practice from the entropy via $S_{\text{imp}}(T_{\text{FL}}) = \frac{1}{4} \ln(2)$, which as such characterizes the flow to the ultimate stable FL FP, and hence complete screening of the impurity spin. T_{FL}/D is shown versus $\rho\delta_K$ for chains of length $N_c = 1, 3, 5, 7$. The dashed lines in the main panel show comparison to the perturbative result for T_K^{SC} given in Eq. (9) [with a prefactor $O(1)$ for each N_c adjusted to fit the numerics]. The inset shows the same data on a log-log scale, demonstrating the quadratic decay of T^* , given by Eq. (13) in the small- $|\delta_K|$ regime (solid lines).

B. Weak interimpurity coupling

The perturbative derivation of the effective 2CK model in Sec. II A 1 is valid for sufficiently large interimpurity exchange couplings, in which regard we note that any bare energy scale larger than the exponentially small universal scales T_K^{2CK} or T_{FL} may be considered “large.”

However, in the $J = 0$ limit, the physical behavior is clearly very different. Here, each terminal spin- $\frac{1}{2}$ impurity undergoes the standard *single-channel* Kondo effect¹⁹ with its attached $\alpha = L/R$ lead below a temperature $T \sim T_{K,\alpha}^{\text{1CK}}$, while the remaining impurities remain free down to $T = 0$. This scale is associated with the flow to the strong coupling (SC) FP,¹⁹ and is given from perturbative scaling¹⁹ by

$$T_{K,\alpha}^{\text{1CK}} \sim D\sqrt{\rho J_{K\alpha}} \exp(-1/\rho J_{K\alpha}). \quad (14)$$

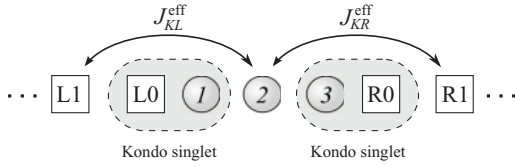


FIG. 9. Schematic illustration for the $N_c = 3$ chain with small interimpurity coupling $J \lesssim T_{K,\alpha}^{\text{ICK}}$, as discussed in the text.

The question addressed in this section is as follows: what is the physics for odd chains with small but finite AF interimpurity coupling, $J \lesssim T_{K,\alpha}^{\text{ICK}}$?

A physically intuitive picture for the simplest $N_c = 3$ case is depicted schematically in Fig. 9 (and discussed further in Sec. II B 1 below). Impurity “1” forms a single-channel Kondo singlet with the left lead, and impurity “3” likewise with the right lead. A Fermi liquid description then applies, and the remaining states of each lead act as an effective bath of noninteracting electrons that participate in the screening of impurity “2.” A residual AF exchange coupling, mediated via the Kondo singlets, once again yields an effective 2CK model.

The above scenario is supported by the behavior of single-channel systems involving side-coupled quantum dots.^{33–36} In the simplest example of a dot dimer, two-stage Kondo screening is operative in the small interdot coupling regime:³⁴ the dot connected to the lead undergoes a spin- $\frac{1}{2}$ Kondo effect on the scale $T_{K,1}$, while residual AF coupling between the remaining dot and the lead gives rise to a second Kondo effect for $T \sim T_{K,2} (\ll T_{K,1})$, leading thereby to complete screening of both dots on the lowest energy scales.³⁴ Similar mechanisms have been advanced to describe the low-energy behavior of an asymmetric two-channel two-impurity Kondo model²⁴ and a triple quantum dot ring structure.⁴³

In the present context of odd impurity chains coupled to two leads, the most interesting behavior is expected in the L/R -symmetric case. Here the effective coupling to the left and right leads is also symmetric, and hence the 2CK FP must describe the low-energy behavior of the system.

1. Effective 2CK model for $N_c = 3$

Before considering NRG calculations, we first derive the effective 2CK model for the simplest $N_c = 3$ case, using perturbative techniques and scaling arguments and exploiting the Wilson chain representation^{57–59} (see Fig. 9) as natural within an RG framework.

The Wilson chain for lead $\alpha = L/R$ is defined^{57–59} by dividing the band up into logarithmic intervals, $\{\pm D\Lambda^{-n}\}$ ($n = 0, 1, 2, \dots$), and then discretizing it by retaining only the symmetric combination of states within each interval. This Hamiltonian is then tridiagonalized to obtain a linear chain form, with the impurity system coupled at one end.^{57–59} The $N_c = 3$ Hamiltonian may thus be written in a dimensionless form $H_N = H_0 + H_1$,

$$\begin{aligned} H_0 &= \mathcal{J}_{KL} \hat{\mathbf{S}}_1 \cdot \hat{\mathbf{S}}_{L0} + \mathcal{J}_{KR} \hat{\mathbf{S}}_3 \cdot \hat{\mathbf{S}}_{R0}, \\ H_1 &= \mathcal{J} (\hat{\mathbf{S}}_1 \cdot \hat{\mathbf{S}}_2 + \hat{\mathbf{S}}_2 \cdot \hat{\mathbf{S}}_3) \\ &+ \sum_{\alpha,\sigma} \sum_{n=0}^{N-1} t_n (f_{\alpha n \sigma}^\dagger f_{\alpha(n+1)\sigma} + f_{\alpha(n+1)\sigma}^\dagger f_{\alpha n \sigma}), \end{aligned} \quad (15)$$

where $\hat{\mathbf{s}}_{\alpha 0}$ is given in Eq. (2) and the Wilson chain operators $f_{\alpha n \sigma}^\dagger$ are obtained recursively using the Lanczos algorithm.⁵⁷ The rescaled dimensionless couplings are given by $\mathcal{J}_{K\alpha} = 2\rho J_{K\alpha}/A_N$ and $\mathcal{J} = 2\rho J/A_N$ [where $A_N = \frac{1}{2}(1 + \Lambda^{-1})\Lambda^{-(N-1)/2}$]. For a flat-band lead density of states, the tunnel-coupling between Wilson chain orbitals takes the form⁵⁷ $t_n = \Lambda^{(N-1)/2} \Lambda^{-n/2} \xi_n$, with the $\xi_n \equiv \xi_n(\Lambda) \sim O(1)$. The full Hamiltonian is then recovered in the $N \rightarrow \infty$ limit^{57–59} via $H = \lim_{N \rightarrow \infty} \{DA_N H_N\}$.

We consider first the limit of strong impurity-lead coupling, $\mathcal{J}_{K\alpha} \gg \max(\mathcal{J}, t_n)$, so that H_0 in Eq. (15) favors the formation of a pair of singlet states between the terminal impurities and the “0” orbital of their attached lead. The ground state of H_0 thus comprises a 1-“L0” singlet (we denote it by $|s; L\rangle$) and a 3-“R1” singlet (denoted $|s; R\rangle$), as shown schematically in Fig. 9.

H_1 now acts perturbatively, and we project onto the lowest state of H_0 using the unity operator for the reduced Hilbert space, $\hat{1}_s = |s; L\rangle\langle s; R| + |s; R\rangle\langle s; L|$. An effective Hamiltonian may be obtained using the Brillouin-Wigner perturbation expansion,⁷⁵ $H_N = E_0 + H_I^{\text{eff}} + H_{\text{II}}^{\text{eff}} + H_{\text{III}}^{\text{eff}} + \dots$. Here, $E_0 = \hat{1}_s H_0 \hat{1}_s = -\frac{3}{4}(\mathcal{J}_{KL} + \mathcal{J}_{KR})$ is merely a constant shift in energy, while $H_I^{\text{eff}} = \hat{1}_s H_1 \hat{1}_s \equiv \tilde{H}_L$ follows as

$$\tilde{H}_L = \sum_{\sigma,\alpha} \sum_{n=1}^{N-1} t_n (f_{\alpha n \sigma}^\dagger f_{\alpha(n+1)\sigma} + f_{\alpha(n+1)\sigma}^\dagger f_{\alpha n \sigma}) \quad (16)$$

and corresponds to a pair of free Wilson chains, with the “0” orbital of each removed. The second-order term, $H_{\text{II}}^{\text{eff}}$, contributes only potential scattering,¹⁹ here omitted for clarity. An effective coupling between impurity “2” and the “L1” and “R1” orbitals is generated only to *third-order* in H_1 , given⁷⁵ by $H_{\text{III}}^{\text{eff}} = \hat{1}_s H_1 (E_0 - H_0)^{-1} \hat{P} H_1 (E_0 - H_0)^{-1} \hat{P} H_1 \hat{1}_s$, with $\hat{P} = \hat{1} - \hat{1}_s$ a projector. Combining this with Eq. (15), a rather lengthy calculation yields

$$H_{\text{III}}^{\text{eff}} = \rho \mathcal{J}_{KL}^{\text{eff}} \hat{\mathbf{S}}_2 \cdot \hat{\mathbf{S}}_{L1} + \rho \mathcal{J}_{KR}^{\text{eff}} \hat{\mathbf{S}}_2 \cdot \hat{\mathbf{S}}_{R1} \quad (17)$$

(omitting RG irrelevant terms), with the effective coupling of impurity “2” to the $\alpha = L/R$ lead given by

$$\rho \mathcal{J}_{K\alpha}^{\text{eff}} = \left(\frac{20t_0^2 \mathcal{J}}{9\mathcal{J}_{K\alpha}^2} \right) > 0. \quad (18)$$

The effective model $H_N^{\text{eff}} = \tilde{H}_L + H_{\text{III}}^{\text{eff}}$ describes thereby the residual AF coupling between impurity “2” and the “L1” and “R1” orbitals of a pair of leads (with impurities “1” and “3” and lead orbitals “L0” and “R0” removed); see Fig. 9. This is a model of 2CK form.

The above analysis presupposes the existence of the local singlet states $|s; L\rangle$ and $|s; R\rangle$. However, we note that for $J \lesssim T_{K,\alpha}^{\text{ICK}}$ [as given by Eq. (14)], RG flow is expected near a Fermi-liquid-type FP, comprising single-channel strong-coupling states in each lead, with a free, disconnected local moment on impurity “2” (and which “SC \times SC \times LM” FP is of course stable only at the point $J = 0$). Renormalization of the impurity-lead coupling $J_{K\alpha} \rightarrow \tilde{J}_{K\alpha}$ on successive reduction of the temperature and energy scales naturally results in incipient formation of Kondo singlets between each terminal impurity and its attached lead below $T \sim T_{K,\alpha}^{\text{ICK}}$ for the $\alpha = L/R$ channel, respectively. An effective 2CK model should then

result via the mechanism described above, where the local singlet states $|s; L\rangle$ and $|s; R\rangle$ are now *Kondo* singlets.

The central question then is as follows: how does Eq. (18) flow under renormalization? Specifically, what is the effective coupling $\rho\tilde{J}_{K,\alpha}^{\text{eff}}$ for $T \sim T_{K,\alpha}^{\text{1CK}}$?

To answer this, recall first that the effective temperature^{57–59} within the RG framework is related to the iteration-number or Wilson chain length, N , via $T \sim \Lambda^{-N/2}$. The operators for the Wilson chain orbitals also scale with N . In particular, operators for the “0” orbital of the Wilson chain scale as^{57,58} $f_{\alpha 0\sigma} \sim \Lambda^{-N/4}$. Thus $\mathcal{J}_{K\alpha} \rightarrow \tilde{\mathcal{J}}_{K\alpha} \sim \Lambda^{-N/2}$, since the impurity-lead exchange coupling is associated with a pair of “0” orbital fermionic operators. The key result is thus that the renormalized impurity-lead coupling $\tilde{\mathcal{J}}_{K\alpha} \sim T_{K,\alpha}^{\text{1CK}}$ for $T \sim T_{K,\alpha}^{\text{1CK}}$ —in accord with the physical expectation that disruption of the $\alpha = L/R$ Kondo singlet costs an energy $O(T_{K,\alpha}^{\text{1CK}})$. By contrast, the coupling between the impurities, \mathcal{J} , is not associated with any chain operators, and hence does *not* get renormalized with N . Further, as pointed out in Ref. 76, once the “0” orbital of a Wilson chain has been frozen out (e.g., by the formation of a Kondo singlet), the “1” orbital operators then scale as $f_{\alpha 1\sigma} \sim \Lambda^{-N/4}$. Thus the renormalized tunnel-coupling $\tilde{t}_0 \sim \Lambda^{-N/4}$, so that for $T \sim T_{K,\alpha}^{\text{1CK}}$, $\tilde{t}_0^2/\tilde{\mathcal{J}}_{K\alpha}$ remains $O(1)$. From Eq. (18), the renormalized effective Kondo coupling at $T \sim T_{K,\alpha}^{\text{1CK}}$ can then be estimated to have the functional dependence $\rho\tilde{J}_{K,\alpha}^{\text{eff}} \sim J/T_{K,\alpha}^{\text{1CK}}$.

For simplicity, we focus now on the mirror-symmetric case, where $J_{K\alpha} \equiv J_K$ and $T_{K,\alpha}^{\text{1CK}} \equiv T_K^{\text{1CK}}$, from which one has the effective low-energy Hamiltonian for $N_c = 3$,

$$H_{N_c}^{\text{eff}} = \tilde{H}_L + \rho\tilde{J}_{K,N_c}^{\text{eff}} \hat{\mathbf{S}} \cdot (\hat{\mathbf{S}}_{L1} + \hat{\mathbf{S}}_{R1}), \quad (19)$$

with $\hat{\mathbf{S}} \equiv \hat{\mathbf{S}}_2$ and the effective coupling

$$\rho\tilde{J}_{K,N_c}^{\text{eff}} = \left(\frac{J}{T_K^{\text{1CK}}} \right) x(N_c) \quad (20)$$

valid for $T \lesssim T_K^{\text{1CK}}$. Determination of the constant $x(N_c)$ is obviously beyond the scope of this analysis, although it can be deduced directly from NRG calculations as demonstrated in the next section.

2CK physics is thus expected for $T \sim T_K^{\text{2CK}} (\ll T_K^{\text{1CK}})$, as given from perturbative scaling¹ by

$$T_K^{\text{2CK}} \sim T_K^{\text{1CK}} \rho\tilde{J}_{K,N_c}^{\text{eff}} \exp(-1/\rho\tilde{J}_{K,N_c}^{\text{eff}}), \quad (21)$$

where the physical origin of the prefactor T_K^{1CK} is simply that the effective bandwidth of the problem is already reduced to $\sim T_K^{\text{1CK}}$ at the temperature $T \sim T_K^{\text{1CK}}$, below which the effective model, Eq. (19), is valid.

2. NRG results for odd chains

The physical picture for the $N_c = 3$ system is thus clear, and we now turn to NRG results for odd chains of length $N_c = 3, 5, 7$ in the regime of weak coupling between the impurities. For accurate numerics, we found it necessary to retain $N_s = 4000, 6000$, and 12000 states per iteration for $N_c = 3, 5$, and 7 , since higher-energy chain states remain important down to $T \sim J \lesssim T_K^{\text{1CK}}$.

Figure 10(A) shows $S_{\text{imp}}(T)$ versus T/D for the $N_c = 3$ case discussed explicitly above, for a common ρJ_K and with

$\rho J = \lambda(T_K^{\text{1CK}}/D)$, where $\lambda = 10^{-n/10}$ and $n = 0, 5, 7, 9, 11, 13$ [lines (a)–(f)]. T_K^{1CK} was itself determined from a $J = 0$ calculation which, modulo a free spin on impurity 2, is equivalent to two separate single-channel Kondo models with the same J_K . At high T , the trivial $S_{\text{imp}} = 3 \ln(2)$ behavior expected for three free spins- $\frac{1}{2}$ arises in all cases. Line (a) crosses directly to $S_{\text{imp}} = \frac{1}{2} \ln(2)$ on the scale $J = T_K^{\text{1CK}} \approx T_K^{\text{2CK}}$, characterizing flow to the 2CK FP. In contrast, lines (b)–(f) flow first to the SC \times SC \times LM FP [$S_{\text{imp}} = \ln(2)$]. We also show for comparison $S_{\text{imp}}^{J=0}(T) = \ln(2) + 2S_{\text{imp}}^{\text{1CK}}(T)$ (diamonds), where $S_{\text{imp}}^{\text{1CK}}(T)$ is the entropy of a single-channel Kondo model¹⁹ with the same Kondo coupling; $S_{\text{imp}}^{J=0}(T)$ thus describes the *entire* temperature dependence of the entropy for $J = 0$. Lines (c)–(f) follow this curve perfectly for $T \gg T_K^{\text{2CK}}$, as expected from the single-channel Kondo screening of impurities “1” and “3”. An intermediate $S_{\text{imp}} = \ln(2)$ plateau is thus observed, the single-channel T_K^{1CK} remaining constant while the two-channel scale T_K^{2CK} diminishes rapidly as J is decreased. RG flow thus persists in the vicinity of the SC \times SC \times LM FP over an extended T range, but below $T \sim T_K^{\text{2CK}}$ all systems are described by the 2CK FP, with residual entropy $S_{\text{imp}} = \frac{1}{2} \ln(2)$.

We now comment on the generic behavior expected for impurity chains with $N_c > 3$, which is a physically natural extension of the $N_c = 3$ case above. Following the “removal” of the terminal impurities through the formation of single-channel Kondo singlets for $T \sim T_K^{\text{1CK}}$, the remaining odd ($N_c - 2$) impurities form a residual spin- $\frac{1}{2}$ on the scale $T \sim J (\lesssim T_K^{\text{1CK}})$. This doublet state now feels an effective coupling to the two leads via the mechanism described in Sec. II B 1, but with a further renormalization of the effective Kondo exchange, as expected from the discussion in Sec. II A in the regime of large interimpurity coupling. Extension of the above analysis for $N_c = 3$, which we do not give here, then leads us to expect (as tested below, Fig. 12) that the form Eq. (20) should hold for odd $N_c > 3$, with ratios $x(N_c + 2)/x(N_c = 3)$ which are the same as those inferred from Table I but with two sites excluded from the spin chain (reflecting quenching of the terminal spins “1” and “ N_c ” to form Kondo singlets), i.e., from Table I that $x(N_c = 5) \approx \frac{2}{3}x(N_c = 3)$ and $x(N_c = 7) \approx 0.51x(N_c = 3)$.

2CK physics is thus expected for all odd chains in the small interimpurity coupling regime below T_K^{2CK} , as given by Eqs. (21) and (20). This is confirmed in Fig. 10(B), where we consider chains of length $N_c = 3, 5, 7$, taking $J = \frac{1}{2}T_K^{\text{1CK}}$ as an illustrative example. Again, at the highest temperatures $T \gg J$, one obtains $S_{\text{imp}} = N_c \ln(2)$. For sufficiently large separation between T_K^{1CK} and J , one expects the entropy to drop first to $S_{\text{imp}} = (N_c - 2) \ln(2)$ on the scale T_K^{1CK} (due to single-channel Kondo quenching¹⁹ of the terminal impurities), followed by a further drop for $T \sim J$ to the LM value $S_{\text{imp}} = \ln(2)$, although in Fig. 10(B), T_K^{1CK} and J are comparable, so no distinct $(N_c - 2) \ln(2)$ plateau arises. In all cases, however, $S_{\text{imp}} = \frac{1}{2} \ln(2)$ is seen below T_K^{2CK} , characteristic of flow to the stable 2CK FP,¹⁴ with scales T_K^{2CK} that evidently diminish with increasing N_c , as expected qualitatively from the above discussion. Figure 10(C) shows the scaling curve obtained when results are plotted versus T/T_K^{2CK} (with $n = 9, 11$ chosen

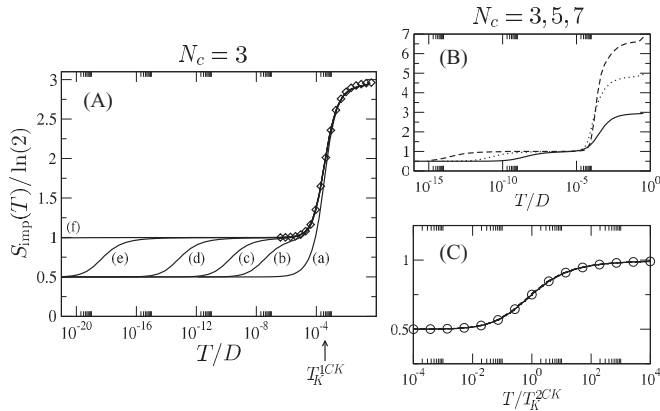


FIG. 10. (A) $S_{\text{imp}}(T)/\ln(2)$ vs T/D as the interimpurity coupling is reduced, for the symmetric $N_c = 3$ case ($\rho\delta_K = 0$). Shown for fixed $\rho J_K = 0.15$, varying $\rho J = \lambda(T_K^{1\text{CK}}/D)$, where $\lambda = 10^{-n/10}$ and $n = 0, 5, 7, 9, 11, 13$ [lines (a)–(f)], with $T_K^{1\text{CK}}$ determined from a $J = 0$ calculation. Behavior for $T \gg T_K^{2\text{CK}}$ is described by $S_{\text{imp}}^{J=0}(T) = \ln(2) + 2S_{\text{imp}}^{1\text{CK}}(T)$ (diamonds), with $S_{\text{imp}}^{1\text{CK}}(T)$ for a single-channel Kondo model with the same J_K . (B) Comparison of behavior for $N_c = 3, 5, 7$ (solid, dotted, and dashed lines) with $J = \frac{1}{2}T_K^{1\text{CK}}$. (C) Results for $N_c = 3, 5, 7$ (with $n = 9$ and 11): scaling collapse to the universal 2CK curve (circles) is seen in all cases.

to ensure good scale separation between $T_K^{2\text{CK}}$ and $T_K^{1\text{CK}}$). The universal curve is precisely that of the standard 2CK model (circles).

Dynamics are now considered briefly, Fig. 11(A) showing the $T = 0$ $D\rho_K(\omega)$ for $N_c = 3$ chains with the same parameters as in Fig. 10(A). All systems show RG flow in the vicinity of the Fermi-liquid-type $\text{SC} \times \text{SC} \times \text{LM}$ FP (reflecting single-channel Kondo screening of the terminal impurities), and hence an incipient single-channel Kondo resonance¹⁹ in each channel. For comparison, we show $D\rho_K^{1\text{CK}}(\omega)$ for a standard single-channel Kondo model with the same spectral coupling (diamonds), which recovers perfectly the spectral behavior for $|\omega| \gg T_K^{2\text{CK}}$. In particular, for lines (d)–(f) in the range $T_K^{2\text{CK}} \ll |\omega| \ll T_K^{1\text{CK}}$, characteristic FL behavior¹⁹ $D\rho_K(\omega) = 1 - a(|\omega|/T_K^{1\text{CK}})^2$ arises, and thus the unitarity limit $D\rho_K(\omega) = 1$ is reached in this intermediate energy window. For any finite J , $T_K^{2\text{CK}}$ is, however, always finite, so ultimately RG flow to the stable 2CK FP yields $D\rho_K(\omega) = \frac{1}{2}$ for $|\omega| \ll T_K^{2\text{CK}}$.

Figure 11(B) shows spectra for $N_c = 3, 5, 7$ chains with common $J = \frac{1}{2}T_K^{1\text{CK}}$, as in Fig. 10(B). These display the same qualitative behavior as for $N_c = 3$, with a single-channel Kondo resonance appearing at $|\omega| \sim T_K^{1\text{CK}}$, before crossing over to the 2CK FP for $|\omega| \sim T_K^{2\text{CK}}$. Since $T_K^{2\text{CK}}$ diminishes with increasing chain length, while $T_K^{1\text{CK}}$ remains fixed, apparent FL behavior consequently persists down to lower energies for the longer chains.

For $N_c = 3, 5, 7$ chains with the same couplings as in Fig. 10(C) and Fig. 11(C) shows the spectrum arising when results are shown versus $\omega/T_K^{2\text{CK}}$: collapse to a single universal scaling curve is seen clearly. One might naively expect to obtain the 2CK scaling spectrum here, since in this regime an effective 2CK model [Eq. (19)] describes the system. However, this model is only valid after the single-channel Kondo effect

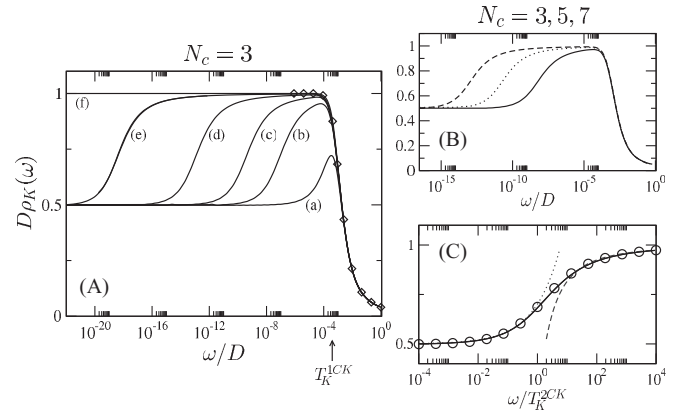


FIG. 11. (A) Spectra $D\rho_K(\omega)$ vs ω/D as the interimpurity coupling is reduced, for the symmetric $N_c = 3$ case (with the same parameters as Fig. 10). Behavior at $|\omega| \gg T_K^{2\text{CK}}$ is described by $D\rho_K^{1\text{CK}}(\omega)$ (diamond points) for a single-channel Kondo model. (B) Comparison of $N_c = 3, 5, 7$ (solid, dotted, dashed lines) with $J = \frac{1}{2}T_K^{1\text{CK}}$. (C) Spectra vs $\omega/T_K^{2\text{CK}}$ for $N_c = 3, 5, 7$ with $n = 9$ and 11: universal scaling collapse is seen. For $T_K^{2\text{CK}} \ll |\omega| \ll T_K^{1\text{CK}}$, the asymptotic behavior is $D\rho_K(\omega) = 1 - A/[\ln^2(|\omega|/T_K^{2\text{CK}}) + B]$ (gray dashed line), while for $|\omega| \ll T_K^{2\text{CK}}$, NFL scaling is observed: $D\rho_K(\omega) = \frac{1}{2}[1 + b(|\omega|/T_K^{2\text{CK}})^{1/2}]$ (gray dotted line). The entire curve is described by $D\rho_K(\omega) = 1 - D\rho_K^{2\text{CK}}(\omega)$ (circles), with $\rho_K^{2\text{CK}}(\omega)$ the scaling spectrum of the standard 2CK model.

has already taken place in each lead, conferring a phase shift of $\pi/2$ to the conduction electrons.¹⁹ As a consequence, the scaling spectrum in the small- J limit is $D\rho_K(\omega) = 1 - D\rho_K^{2\text{CK}}(\omega)$, with $D\rho_K^{2\text{CK}}(\omega)$ the scaling spectrum of the regular single-spin 2CK model. Comparison with the latter (circles) confirms this directly.

Finally, in Fig. 12 we analyze the variation of the two-channel Kondo scale as a function of the interimpurity coupling strength, ρJ , and the chain length, N_c . The $T_K^{2\text{CK}}/D$ in the

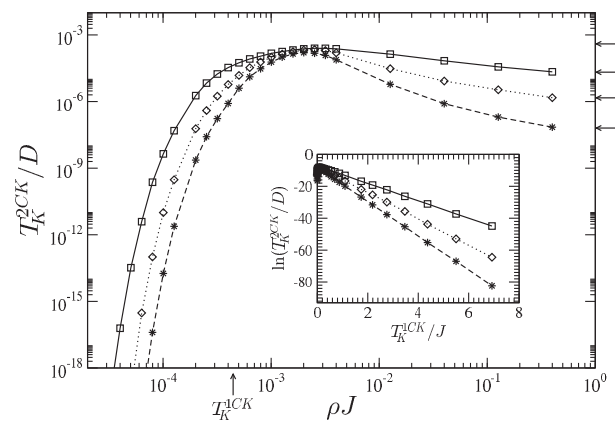


FIG. 12. Evolution of the two-channel Kondo scale: $T_K^{2\text{CK}}/D$ vs ρJ for symmetric chains of length $N_c = 3, 5, 7$ (squares, diamonds, and stars), and Kondo coupling $\rho J_K = 0.15$ (with $\delta_K = 0$). For large interimpurity coupling, $T_K^{2\text{CK}}$ is given by Eqs. (7) and (8) (indicated by arrows). For each chain, the maximum value $T_K^{2\text{CK}} \approx T_K^{1\text{CK}}$ is obtained for $J \approx 10T_K^{1\text{CK}}$. For $J < T_K^{1\text{CK}}$, the Kondo scale diminishes rapidly, as is seen also in the inset, where $\ln(T_K^{2\text{CK}})$ vs $T_K^{1\text{CK}}/J$ is shown, confirming Eqs. (20) and (21). The slopes yield $x(N_c = 3) \approx 1/6$, $x(N_c = 5) \approx 1/9$, and $x(N_c = 7) \approx 1/12$.

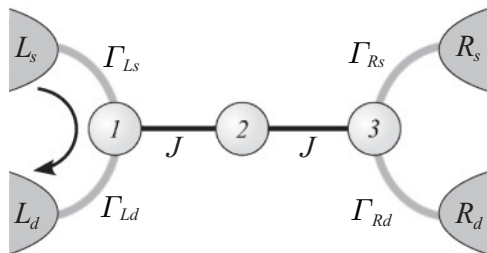


FIG. 13. Schematic of the $N_c = 3$ trimer with impurities “1” and “3” modeled as Anderson-like correlated levels, each tunnel-coupled to both source (s) and drain (d) leads, with hybridizations $\Gamma_{\alpha\gamma}$ (where $\alpha = L/R$ and $\gamma = s/d$). The impurities are exchange-coupled to eliminate $L \leftrightarrow R$ charge-transfer processes that destroy 2CK physics, but conductance through impurity 1 (3) in channel $\alpha = L (R)$ can be measured.

large- J limit (indicated by arrows) are in accord with Eqs. (7) and (8). However, as ρJ is decreased, $T_K^{2\text{CK}}$ first increases (reaching its maximum of $T_K^{2\text{CK}} \approx T_K^{1\text{CK}}$ for $J \approx 10T_K^{1\text{CK}}$ in each case), then diminishes very rapidly for $J \ll T_K^{1\text{CK}}$. The behavior for small interimpurity coupling is seen most clearly in the inset, where $\ln(T_K^{2\text{CK}}/D)$ is shown versus $T_K^{1\text{CK}}/J$. The linear behavior confirms Eqs. (20) and (21), with the slopes yielding $x(N_c = 3) \approx 1/6$, $x(N_c = 5) \approx 1/9$, and $x(N_c = 7) \approx 1/12$, as is consistent with the expectation discussed above.

III. GATE VOLTAGE EFFECTS AND CONDUCTANCE

Having analyzed in detail the Heisenberg chain model, Eq. (1), we now consider a variant in which the terminal impurities are treated as correlated *levels* (dots), tunnel-coupled to their respective leads. Each lead $\alpha = L$ and R can be “split” into source (s) and drain (d), allowing the conductance through dot “1” (or “ N_c ”) to be measured; see Fig. 13. The Hamiltonian we study is $\mathcal{H}^{N_c} = \mathcal{H}_L + \mathcal{H}_c^{N_c} + \mathcal{H}_{\text{hyb}}^{N_c}$, where the four equivalent noninteracting leads are given by

$$\mathcal{H}_L = \sum_{\alpha = L/R} \sum_{\gamma = s/d} \sum_{\mathbf{k}, \sigma} \epsilon_{\mathbf{k}} c_{\alpha\gamma\mathbf{k}\sigma}^\dagger c_{\alpha\gamma\mathbf{k}\sigma}, \quad (22)$$

and the impurity chain is described by

$$\begin{aligned} \mathcal{H}_c^{N_c} = & J \sum_{i=1}^{N_c-1} \hat{\mathbf{S}}_i \cdot \hat{\mathbf{S}}_{i+1} \\ & + U(\hat{n}_{1\uparrow}\hat{n}_{1\downarrow} + \hat{n}_{N_c\uparrow}\hat{n}_{N_c\downarrow}) + \epsilon(\hat{n}_1 + \hat{n}_{N_c}), \end{aligned} \quad (23)$$

where $\hat{n}_i = \sum_{\sigma} \hat{n}_{i\sigma} = \sum_{\sigma} d_{i\sigma}^\dagger d_{i\sigma}$ is the number operator for dot $i = 1$ or N_c , ϵ is its level energy, and U is its Coulomb repulsion (charging energy). In a real quantum dot device, the level energy is proportional to the gate voltage, $\epsilon \propto V_g$. The leads and chain are coupled via

$$\mathcal{H}_{\text{hyb}}^{N_c} = \sum_{\gamma = s/d} \sum_{\mathbf{k}, \sigma} (V_{L\gamma} c_{L\gamma\mathbf{k}\sigma}^\dagger d_{1\sigma} + V_{R\gamma} c_{R\gamma\mathbf{k}\sigma}^\dagger d_{N_c\sigma} + \text{H.c.}), \quad (24)$$

where $V_{\alpha\gamma}$ is the tunnel-coupling matrix element for the $\alpha = L/R$ and $\gamma = s/d$ lead. The hybridization strength follows as $\Gamma_{\alpha\gamma} = \pi\rho_T V_{\alpha\gamma}^2$ (with $\rho_T = N\rho$ the total lead density of states as before). Finally, a simple canonical transformation of the lead orbitals, via

$$\begin{aligned} c_{\alpha s\mathbf{k}\sigma} &= a_{\alpha\mathbf{k}\sigma} \cos(\theta_\alpha) + \tilde{a}_{\alpha\mathbf{k}\sigma} \sin(\theta_\alpha), \\ c_{\alpha d\mathbf{k}\sigma} &= a_{\alpha\mathbf{k}\sigma} \sin(\theta_\alpha) - \tilde{a}_{\alpha\mathbf{k}\sigma} \cos(\theta_\alpha), \end{aligned} \quad (25)$$

with $\tan(\theta_\alpha) = V_{\alpha d}/V_{\alpha s}$, yields an effective *two-channel* model with

$$H_L = \sum_{\alpha, \mathbf{k}, \sigma} \epsilon_{\mathbf{k}} a_{\alpha\mathbf{k}\sigma}^\dagger a_{\alpha\mathbf{k}\sigma}, \quad (26a)$$

$$\mathcal{H}_{\text{hyb}}^{N_c} = \sum_{\mathbf{k}, \sigma} (V_L a_{L\mathbf{k}\sigma}^\dagger d_{1\sigma} + V_R a_{R\mathbf{k}\sigma}^\dagger d_{N_c\sigma} + \text{H.c.}), \quad (26b)$$

where $V_\alpha^2 = V_{\alpha s}^2 + V_{\alpha d}^2$, so that in particular for $V_L^2 = V_R^2 \equiv V^2$ (and hence $\Gamma_L = \Gamma_R \equiv \Gamma = \pi\rho_T V^2$) the model is mirror-symmetric. To investigate 2CK physics on the lowest energy scales, this is the situation now considered. We also focus on the simplest example of the $N_c = 3$ trimer, variants of which have been studied recently in certain parameter regimes,^{38–45} including exchange-coupled chain⁴² and ring^{43,45} structures at half-filling. As shown below, a physically intuitive perturbative treatment of the model for different fillings yields effective 2CK models—in spin and orbital sectors—from which the gate voltage dependence of the 2CK scale can be identified.

A. Effective low-energy models for $N_c = 3$

In the atomic limit ($V = 0$) of the isolated $N_c = 3$ trimer, the number of chain electrons jumps discontinuously between integer values $\mathcal{N} = n_1 + n_3 + 1 = 1 \rightarrow 5$ as the gate voltage $V_g \propto \epsilon$ is varied (recall that impurity “2” is a strict spin- $\frac{1}{2}$). On tunnel-coupling to the leads, this Coulomb-blockade (CB) staircase is naturally smoothed into a continuous crossover. Regimes of occupancy can still, however, be identified, and sufficiently deep within the CB valleys, \mathcal{N} will be approximately integral. Here, a full $O(V^2)$ Schrieffer-Wolff (SW) transformation^{19,77} can be performed in the strongly correlated regime of interest $U \gg V$, perturbatively eliminating virtual excitations into high-energy manifolds with $(\mathcal{N} \pm 1)$ chain electrons.

In the atomic limit, the ground state in any given \mathcal{N} -electron sector is a doublet, which we denote $|\mathcal{N}; \pm \frac{1}{2}\rangle$. Projecting onto the reduced (chain) Hilbert space of this doublet using the unity operator

$$\hat{1}_{\mathcal{N}} = \sum_{\gamma = \pm \frac{1}{2}} |\mathcal{N}; \gamma\rangle \langle \mathcal{N}; \gamma| \quad (27)$$

yields an effective model $\mathcal{H}_{\mathcal{N}}^{\text{eff}} = H_L + \mathcal{H}_{\mathcal{N},\text{II}}^{\text{eff}}$, where the leading $O(V^2)$ contribution arising from tunnel coupling to the leads [Eq. (26b) with $V_L = V_R$ and $N_c = 3$, denoted as \mathcal{H}^{I}] is given by the SW transformation^{19,77}

$$\mathcal{H}_{\mathcal{N},\text{II}}^{\text{eff}} = \hat{1}_{\mathcal{N}} \mathcal{H}^{\text{I}} (E_0 - \mathcal{H}_c^{N_c=3})^{-1} \mathcal{H}^{\text{I}} \hat{1}_{\mathcal{N}}. \quad (28)$$

Here $E_0 = \hat{1}_{\mathcal{N}} \mathcal{H}_c^{N_c=3} \hat{1}_{\mathcal{N}}$ is the energy of the ground chain doublet (and retardation has as usual been neglected¹⁹).

In the following, we also exploit the particle-hole transformation

$$\begin{aligned} d_{i\sigma} &\rightarrow d_{i\sigma}^\dagger, & a_{\alpha\mathbf{k}\sigma} &\rightarrow -a_{\alpha-\mathbf{k}\sigma}^\dagger, \\ \hat{S}_2^\pm &\rightarrow -\hat{S}_2^\mp, & \hat{S}_2^z &\rightarrow -\hat{S}_2^z, \end{aligned} \quad (29)$$

which yields directly $\hat{N} \rightarrow (6 - \hat{N})$. The full Hamiltonian [parametrized by $\mathcal{H} \equiv \mathcal{H}(\epsilon)$ for given U , J , and V] transforms as $\mathcal{H}(\epsilon) \rightarrow \mathcal{H}(-\epsilon - U) + (2U - 4\epsilon)$. In general, the physical behavior of $\mathcal{H}(\epsilon)$ and $\mathcal{H}(-\epsilon - U)$ is equivalent, since the constant shift $(2U - 4\epsilon)$ is irrelevant in the calculation of observable quantities. Thus, the $\mathcal{N} = 1 \leftrightarrow 5$ and $\mathcal{N} = 2 \leftrightarrow 4$ sectors are related by the reflection about the particle-hole symmetric point $\epsilon = -\frac{1}{2}U$. Together with the singly occupied ($\mathcal{N} = 3$)-electron case, three distinct regions of electron filling must arise as a consequence. We now consider them in turn.

1. ($\mathcal{N} = 3$)-electron regime

For $-(U + \frac{1}{4}J) < \epsilon < \frac{1}{4}J$, the atomic limit trimer ground state is a singly occupied spin doublet⁴⁵

$$|\mathcal{N} = 3; S^z\rangle = \frac{\sigma}{\sqrt{6}} \left[\hat{S}_2^\sigma (d_{1\uparrow}^\dagger d_{3\downarrow}^\dagger - d_{3\uparrow}^\dagger d_{1\downarrow}^\dagger) - 2\hat{S}_2^{-\sigma} d_{1\sigma}^\dagger d_{3\sigma}^\dagger \right] |\text{vac}\rangle, \quad (30)$$

where $S^z = \frac{\sigma}{2}$ with $\sigma = \pm$ for spins \uparrow/\downarrow , and $\hat{S}_2^\sigma \equiv \hat{S}_2^\pm$ is a spin raising (lowering) operator. $|\text{vac}\rangle = \sum_{\sigma_2} |-\sigma_2; -\rangle$ defines the ‘‘vacuum’’ state of the local (chain) Hilbert space, in which dots ‘‘1’’ and ‘‘3’’ are unoccupied, while ‘‘2’’ carries a free spin- $\frac{1}{2}$.

Using Eq. (30) with Eqs. (27) and (28) leads eventually to the effective low-energy model deep in the $\mathcal{N} = 3$ CB valley,

$$\mathcal{H}_{\mathcal{N}=3}^{\text{eff}} = H_L + J_{K,\mathcal{N}=3}^{\text{eff}} \hat{\mathbf{S}} \cdot (\hat{\mathbf{S}}_{L0} + \hat{\mathbf{S}}_{R0}), \quad (31)$$

where we have omitted potential scattering contributions for clarity, and $\hat{\mathbf{S}}$ is a spin- $\frac{1}{2}$ operator for the lowest chain doublet, defined by $\hat{S}^z = \sum_{S^z} |\mathcal{N} = 3; S^z\rangle S^z \langle \mathcal{N} = 3; S^z|$ and $\hat{S}^\pm = |\mathcal{N} = 3; \pm\frac{1}{2}\rangle \langle \mathcal{N} = 3; \mp\frac{1}{2}|$. Equation (31) is of 2CK form, with effective Kondo coupling

$$\rho J_{K,\mathcal{N}=3}^{\text{eff}} = \frac{4\Gamma}{6\pi} \left\{ \frac{9}{J + 4\epsilon + 4U} + \frac{9}{J - 4\epsilon} - \frac{1}{5J + 4\epsilon + 4U} - \frac{1}{5J - 4\epsilon} \right\}, \quad (32)$$

which is AF throughout the entire $\mathcal{N} \approx 3$ sector. In the particle-hole symmetric Kondo limit in particular ($\epsilon = -\frac{1}{2}U$), one obtains $\rho J_{K,\mathcal{N}=3}^{\text{eff}} = \frac{2}{3}\rho J_K$ to leading order in $1/U$ [with $\rho J_K = 8\Gamma/(\pi U)$ the effective exchange coupling of a *single* Anderson impurity¹⁹ tunnel-coupled to leads], which as such is consistent with Eq. (7) and Table I for the $N_c = 3$ Heisenberg chain studied in Sec. II A.

Two-channel Kondo physics thus arises in the $\mathcal{N} \approx 3$ regime, with T_K^{2CK} in particular given from Eqs. (8) and (32).

2. ($\mathcal{N} = 2,4$)-electron regime: Orbital 2CK effect

As above, the ($\mathcal{N} = 2,4$)-electron regimes are related by the particle-hole transformation Eq. (29), so we consider explicitly only the $\mathcal{N} = 4$ case. The $\mathcal{N} = 4$ regime is the

ground state of the free trimer over an ϵ interval of width $J/2$, specifically $-(U + \frac{3}{4}J) < \epsilon < -(U + \frac{1}{4}J)$. The ground state comprises a degenerate pair of spin singlets, since the spin- $\frac{1}{2}$ on impurity ‘‘2’’ can form a local singlet with either ‘‘1’’ or ‘‘3’’ (the remaining site being doubly occupied). Since the states are spin singlets, two-channel *spin*-Kondo physics will obviously not arise here.

The $\mathcal{N} = 4$ states are, however, doubly degenerate, so they may be associated with an orbital pseudospin (\hat{T}) and be expressed as

$$|\mathcal{N} = 4; T^z\rangle = \frac{\sigma}{\sqrt{2}} \left[(\hat{S}_2^- d_{(2+\sigma)\uparrow}^\dagger - \hat{S}_2^+ d_{(2+\sigma)\downarrow}^\dagger) \times d_{(2-\sigma)\uparrow}^\dagger d_{(2-\sigma)\downarrow}^\dagger \right] |\text{vac}\rangle, \quad (33)$$

with $T^z = \frac{\sigma}{2}$ for $\sigma = \pm 1$. Projecting into this reduced Hilbert space using the $\mathcal{N} = 4$ unity operator Eq. (27) with the SW transformation Eq. (28) yields an effective *orbital* 2CK model

$$\mathcal{H}_{\mathcal{N}=4}^{\text{eff}} = H_L + J_{K,\mathcal{N}=4}^{\text{eff}} \hat{\mathcal{T}} \cdot (\hat{\boldsymbol{\tau}}_{0,\uparrow} + \hat{\boldsymbol{\tau}}_{0,\downarrow}), \quad (34)$$

with an effective exchange coupling

$$\rho J_{K,\mathcal{N}=4}^{\text{eff}} = \frac{\Gamma}{2\pi} \left\{ \frac{1}{\epsilon + U - \frac{3}{4}J} + \frac{2}{\epsilon + U + \frac{3}{4}J} - \frac{3}{\epsilon + U + \frac{1}{4}J} \right\}, \quad (35)$$

which is AF within the $\mathcal{N} \approx 4$ regime. The trimer orbital pseudospin $\hat{\mathcal{T}}$ is a spin- $\frac{1}{2}$ operator defined by $\hat{\mathcal{T}}^z = \sum_{T^z} |\mathcal{N} = 4; T^z\rangle T^z \langle \mathcal{N} = 4; T^z|$ and $\hat{\mathcal{T}}^\pm = |\mathcal{N} = 4; \pm\frac{1}{2}\rangle \langle \mathcal{N} = 4; \mp\frac{1}{2}|$. Similarly, we may define a lead pseudospin $\hat{\boldsymbol{\tau}}_{0,\sigma}$ for each real spin $\sigma = \uparrow/\downarrow$ as $\hat{\boldsymbol{\tau}}_{0,\sigma}^z = \frac{1}{2}(f_{L0\sigma}^\dagger f_{L0\sigma} - f_{R0\sigma}^\dagger f_{R0\sigma})$ and $\hat{\boldsymbol{\tau}}_{0,\sigma}^\pm = f_{L0\sigma}^\dagger f_{R0\sigma}$ [with $\hat{\boldsymbol{\tau}}_{0,\sigma}^- = (\hat{\boldsymbol{\tau}}_{0,\sigma}^+)^\dagger$], where $f_{\alpha 0\sigma}^\dagger$ is given by Eq. (2b).

The important ‘‘pseudospin-flip’’ processes embodied in Eq. (34) correspond physically to moving an electron of given real spin from one lead to the other, while simultaneously switching the trimer orbital participating in the local singlet, such that no net charge transfer occurs between leads. Real spin $\sigma = \uparrow/\downarrow$ here plays the role of the channel index, and as such orbital 2CK physics is expected below $T \sim T_K^{\text{2CK}}$, as given by Eq. (8) using the effective coupling Eq. (35).

3. ($\mathcal{N} = 1,5$)-electron regime

For $\epsilon < -(U + \frac{3}{4}J)$, the ground state in the atomic limit lies in the ($\mathcal{N} = 5$)-electron regime. It is a spin doublet, comprising the free spin-1/2 on ‘‘impurity’’ 2, with sites ‘‘1’’ and ‘‘3’’ each doubly occupied: $|\mathcal{N} = 5; S^z\rangle = \hat{S}_2^\sigma d_{1\uparrow}^\dagger d_{1\downarrow}^\dagger d_{3\uparrow}^\dagger d_{3\downarrow}^\dagger |\text{vac}\rangle$. Virtual excitations to the ($\mathcal{N} = 4$)-electron sectors are perturbatively eliminated to $O(V^2)$ by the SW transformation [Eq. (28)], leading to

$$\mathcal{H}_{\mathcal{N}=5}^{\text{eff}} = H_L + J_{K,\mathcal{N}=5}^{\text{eff}} \hat{\mathbf{S}}_2 \cdot (\hat{\mathbf{S}}_{L0} + \hat{\mathbf{S}}_{R0}), \quad (36)$$

with effective coupling

$$\rho J_{K,\mathcal{N}=5}^{\text{eff}} = \frac{\Gamma}{\pi} \left\{ \frac{1}{\epsilon + U - \frac{1}{4}J} - \frac{1}{\epsilon + U + \frac{3}{4}J} \right\}, \quad (37)$$

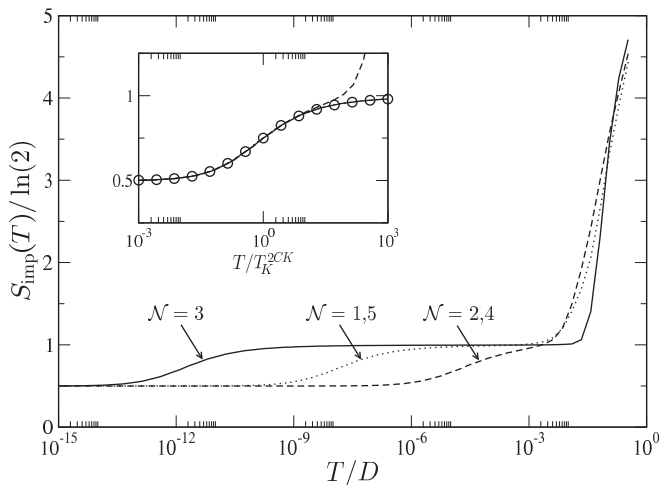


FIG. 14. Entropy $S_{\text{imp}}(T)$ vs T/D for a trimer with tunnel-coupled leads. Shown for $\rho J = 0.075$, $U/\pi\Gamma = 10$, and $\Gamma/D = 10^{-2}$, varying $\epsilon/\pi\Gamma = -5, -12.5, -14.5$ (solid, dashed, and dotted lines), respectively, representing systems “deep” in the $\mathcal{N} = 3, 4, 5$ CB valleys. Identical results are obtained for their particle-hole transformed counterparts. Inset: the low-temperature scaling behavior in terms of $T/T_K^{2\text{CK}}$, compared with the standard 2CK model (circles).

which is AF throughout the ($\mathcal{N} \approx 5$)-electron regime. Two-channel spin-Kondo physics is thus again expected below $T \sim T_K^{2\text{CK}}$ [given via Eq. (8)].

B. Thermodynamics and scaling

The physical picture is clear: 2CK physics, whether of spin or orbital character, is expected when sufficiently deep in each region of electron filling. We confirm this directly using NRG for the full trimer model in Fig. 14, where the entropy $S_{\text{imp}}(T)/\ln(2)$ versus T/D is shown for fixed representative ρJ , $U/\pi\Gamma$, and Γ/D , varying $\epsilon/\pi\Gamma$ for systems deep in the ($\mathcal{N} = 3, 4, 5$)-electron CB valleys.

In each case, the high-temperature $T > U$ behavior is simply that of two free orbitals and a free spin, giving $S_{\text{imp}} = 5 \ln(2)$. The LM FP is reached directly as T is lowered, yielding $S_{\text{imp}} = \ln(2)$; flow to the 2CK FP with characteristic¹⁴ $S_{\text{imp}} = \frac{1}{2} \ln(2)$ follows below $T \sim T_K^{2\text{CK}}$. Upon rescaling in terms of $T/T_K^{2\text{CK}}$ (see inset), the systems in each regime of filling collapse to the universal 2CK curve (circles), thus confirming the effective low-energy models Eqs. (31), (34), and (36).

Figure 15 shows the evolution of the 2CK scale as the level energy ($\epsilon \propto V_g$) is varied essentially continuously over a wide range of $\epsilon/\pi\Gamma$, for systems with the same ρJ , $U/\pi\Gamma$, and Γ/D as in Fig. 14. NRG results (points) are compared with the perturbative result for $T_K^{2\text{CK}}$ given in Eq. (8), using the effective Kondo couplings valid in the $\mathcal{N} = 3$ regime [Eq. (32)], the $\mathcal{N} = 2, 4$ regimes [Eq. (35)], and the $\mathcal{N} = 1, 5$ regimes [Eq. (37)]. Throughout the majority of parameter space, the agreement is excellent; only at the boundary between regimes does the perturbative treatment (naturally) break down. Further, while the mechanism for overscreening changes from spin-2CK (odd- \mathcal{N}) to orbital-2CK (even- \mathcal{N}) across these boundaries, $T_K^{2\text{CK}}$ itself is found from NRG to

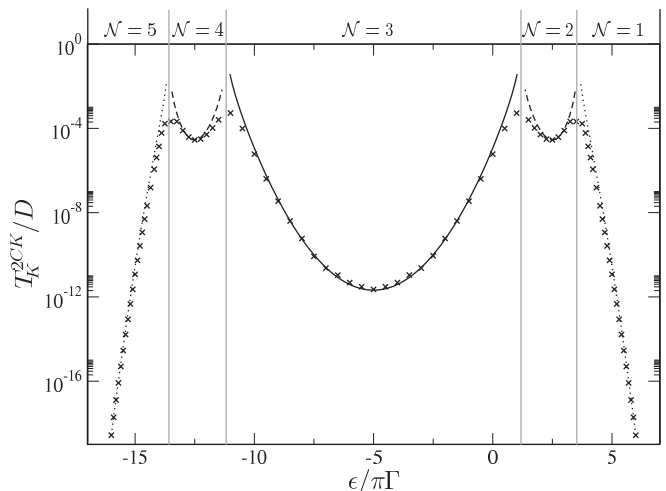


FIG. 15. Evolution of the two-channel Kondo scale $T_K^{2\text{CK}}/D$ vs $\epsilon/\pi\Gamma$ for $\rho J = 0.075$, $U/\pi\Gamma = 10$, and $\Gamma/D = 10^{-2}$. NRG results (points) are compared with Eq. (8) using effective Kondo couplings valid in the $\mathcal{N} = 3$ regime [Eq. (32), solid line], $\mathcal{N} = 2, 4$ regimes [Eq. (35), dashed lines], and the $\mathcal{N} = 1, 5$ regimes [Eq. (37), dotted lines].

vary smoothly, with the 2CK FP remaining the stable FP in all cases (including for $\epsilon/\pi\Gamma < -14$ and $> +4$ in Fig. 15, where $T_K^{2\text{CK}}$ diminishes rapidly but nonetheless remains finite).

C. Single-particle dynamics and conductance

We turn now to dynamics, focusing again on the spectrum $-\pi\rho_T \text{Im}[t_L(\omega)] \equiv \pi\Gamma D_1(\omega)$, where $D_1(\omega) = -\frac{1}{\pi} \text{Im}[G_1(\omega)]$ with G_1 the local retarded Green function for dot “1.” We obtain it through the Dyson equation,

$$[G_1(\omega)]^{-1} = [G_1^0(\omega)]^{-1} - \Sigma_1(\omega), \quad (38)$$

where $G_1^0(\omega)$ is the noninteracting propagator (obtained for $U = 0 = J$), and $\Sigma_1(\omega) = \Sigma_1^R(\omega) - i\Sigma_1^I(\omega)$ is the proper electron self-energy. The noninteracting $G_1^0(\omega)$ is simply¹⁹ $[G_1^0(\omega)]^{-1} = \omega^+ - \epsilon - \Gamma(\omega)$ (with $\omega^+ = \omega + i0^+$), where $\Gamma(\omega) = \Gamma^R(\omega) - i\Gamma^I(\omega)$, with $\Gamma^I(\omega) = \Gamma (= \pi V^2 \rho_T)$ for all $|\omega| < D$ inside the band, and $\Gamma^R(\omega = 0) = 0$.

An expression for $\Sigma_1(\omega)$ is readily obtained using equation of motion methods,^{19,66} and is given by

$$\begin{aligned} \Sigma_1(\omega) = & [G_1(\omega)]^{-1} \{ U \langle \langle d_{1\uparrow} \hat{n}_{1\downarrow}; d_{1\uparrow}^\dagger \rangle \rangle_\omega \\ & + \frac{1}{2} J \langle \langle d_{1\downarrow} \hat{S}_2^- + d_{1\uparrow} \hat{S}_2^z; d_{1\uparrow}^\dagger \rangle \rangle_\omega \}, \end{aligned} \quad (39)$$

where the local Green function itself is $G_1(\omega) = \langle \langle d_{1\sigma}; d_{1\sigma}^\dagger \rangle \rangle_\omega$ [independent of spin σ in the absence of a magnetic field, and with $G_1(\omega) = G_3(\omega)$ in the mirror-symmetric systems considered]. The self-energy can be calculated directly within the density-matrix formulation of NRG^{59–61,67} via Eq. (39), with $G_1(\omega)$ then obtained from Eq. (38). In particular, the local propagator for $\omega = 0$ may be expressed simply as $[G_1(0)]^{-1} = -\epsilon^* + i\Gamma^*$ in terms of the renormalized single-particle level ϵ^* and renormalized hybridization Γ^* , given by

$$\epsilon^* = \epsilon + \Sigma_1^R(0), \quad (40a)$$

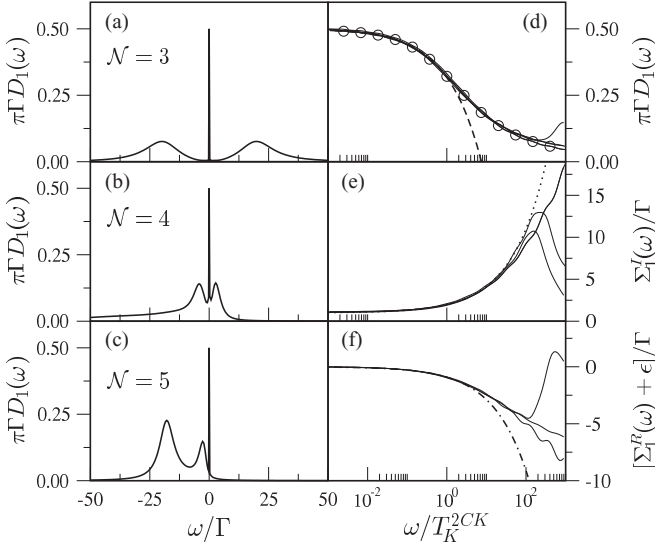


FIG. 16. (a)–(c) $T = 0$ single-particle spectrum $\pi\Gamma D_1(\omega)$ vs ω/Γ . Shown for $\rho J = 0.075$, $U/\pi\Gamma = 10$, $\Gamma/D = 10^{-2}$, with $\epsilon/\pi\Gamma = -5$ [$\mathcal{N} = 3$, panel (a)], -12.5 [$\mathcal{N} \approx 4$, panel (b)], and -14.5 [$\mathcal{N} \approx 5$, panel (c)]. (d) Collapse to the universal 2CK scaling spectrum (circles). The scaling behavior of the proper self-energy, plotted as $\Sigma_1^I(\omega)/\Gamma$ and $[\Sigma_1^R(\omega) + \epsilon]/\Gamma$, is shown in (e) and (f). Asymptotic $|\omega| \ll T_K^{2CK}$ behavior described by $\pi\Gamma D_1(\omega) = \frac{1}{2}[1 - b(|\omega|/T_K^{2CK})^{1/2}]$ (dashed line); $\Sigma_1^I(\omega)/\Gamma = 1 + 2b(|\omega|/T_K^{2CK})^{1/2}$ (dotted line); and $[\Sigma_1^R(\omega) + \epsilon]/\Gamma = -\text{sgn}(\omega)2b(|\omega|/T_K^{2CK})^{1/2}$ (dot-dashed line).

$$\Gamma^* = \Gamma + \Sigma_1^I(0) \quad (40b)$$

in terms of the self-energy at $\omega = 0$. The Fermi level value of the single-particle spectrum then follows as

$$\pi\Gamma D_1(\omega = 0) = \frac{\Gamma}{\Gamma^*} \frac{1}{1 + (\epsilon^*/\Gamma^*)^2}. \quad (41)$$

NRG results are considered in Fig. 16, panels (a)–(c), showing $\pi\Gamma D_1(\omega)$ versus ω/Γ for fillings $\mathcal{N} = 3, 4, 5$, with the same parameters as used in Fig. 14. First, we comment briefly on the high-energy “Hubbard satellites” clearly visible in $D_1(\omega)$. As usual,¹⁹ these reflect simple one-electron addition ($\omega > 0$) or subtraction ($\omega < 0$) from the isolated chain \mathcal{N} -electron ground states. Their locations, broadened somewhat on coupling to the leads, are thus readily understood from the $V = 0$ atomic limit ground states of Sec. III A. Given their simplicity, we do not comment further on them, save to note that in the $\mathcal{N} = 3$ particle-hole symmetric example of panel (a), $D_1(\omega) = D_1(-\omega)$ as expected, and that for the $\mathcal{N} = 5$ example in panel (c), high-energy features are naturally observed only for $\omega < 0$, corresponding to excitations to ($\mathcal{N} = 4$)-electron states.

The most important feature of $D_1(\omega)$ in Fig. 16 is of course the low-energy Kondo resonance, associated with RG flow in the vicinity of the stable 2CK FP. This is shown in panel (d), where spectra from the $\mathcal{N} = 3, 4, 5$ regimes are again shown, but now rescaled in terms of ω/T_K^{2CK} . Collapse to a single curve is seen, with the value at the Fermi level in particular pinned to $\pi\Gamma D_1(\omega = 0) = \frac{1}{2}$, independent of ϵ . The low-

energy asymptotics of the scaling spectrum (dashed line) are found to be

$$\pi\Gamma D_1(\omega) \underset{|\omega| \ll T_K^{2CK}}{\sim} \frac{1}{2} [1 - b(|\omega|/T_K^{2CK})^{1/2}], \quad (42)$$

as consistent with behavior near the 2CK FP discussed in connection with a variety of related two-channel models (see, e.g., Refs. 13,42,45,68–71). Indeed, comparison to the spectrum $D\rho_K(\omega)$ for the 2CK model shows perfect agreement in the low-energy scaling regime. This behavior is in striking contrast to that arising¹⁹ in a FL phase for $|\omega| \ll T_K$: $\pi\Gamma D(\omega) = \sin^2(\delta) - a_1(\omega/T_K) - a_2(\omega/T_K)^2$, describing the approach to the Fermi level value, which itself depends on the phase shift, δ . For the Anderson model,¹⁹ $\delta = \frac{\pi}{2}n_{\text{imp}}$ by the Friedel sum rule,^{19,65} with n_{imp} the “excess” charge in the system induced by addition of the impurity. Thus, $D(\omega = 0)$ depends on the dot filling—and hence on the level energy ϵ —in a regular FL. The situation is clearly quite different in the stable NFL phase obtained for the chain models studied in the present work, and we shall consider the analog of the Friedel sum rule in Sec. III E below.

Further insight is gained, however, from the electron self-energy itself, the imaginary and real parts of which are shown, respectively, in panels (e) and (f) of Fig. 16. To emphasize the low-energy scaling of interest, we show the results for $\mathcal{N} = 3, 4, 5$ in terms of ω/T_K^{2CK} . The common asymptotic form for $|\omega| \ll T_K^{2CK}$ is found to be

$$\Sigma_1^I(\omega)/\Gamma \sim 1 + 2b(|\omega|/T_K^{2CK})^{1/2}, \quad (43a)$$

$$\Sigma_1^R(\omega)/\Gamma \sim -\epsilon/\Gamma - \text{sgn}(\omega)2b(|\omega|/T_K^{2CK})^{1/2} \quad (43b)$$

[with $b \sim O(1)$ precisely the same constant as in Eq. (42)]. At the Fermi level in particular, $\Sigma_1^I(\omega = 0) = \Gamma$, in contrast to generic FL behavior $\Sigma^I(\omega = 0) = 0$. Indeed, extensive examination of NRG results over the entire parameter space confirms Eq. (43) generally—for any value of the bare level energy ϵ , and for all interaction strengths U/Γ and exchange couplings $\rho J > 0$. The renormalized level energy and hybridization then follow from Eq. (40) as $\epsilon^* = 0$ and $\Gamma^* = 2\Gamma$. From Eq. (41), the spectrum at the Fermi level is consequently pinned to a universal half-unity value, $\pi\Gamma D_1(\omega = 0) = \frac{1}{2}$ for all underlying bare parameters, as illustrated in panel (d) of Fig. 16.

I. Conductance

To measure the differential conductance through dot “1,” a bias voltage V_{sd} is applied across the L source and drain leads, inducing a chemical potential difference $\mu_s - \mu_d = eV_{sd}$. The L/R symmetry required to observe 2CK physics on the lowest energy scales also requires of course that the same bias be applied across the R lead. Following Meir and Wingreen,⁷⁸ the zero-bias conductance through dot “1” is given exactly by

$$G_c = \frac{2e^2}{h} G_0 \int_{-\infty}^{\infty} d\omega (-) \frac{\partial f(\omega)}{\partial \omega} \pi\Gamma D_1(\omega), \quad (44)$$

where $D_1(\omega)$ is the single-particle spectrum at equilibrium, $f(\omega) = [e^{\omega/T} + 1]^{-1}$, and $\Gamma = \Gamma_s + \Gamma_d$ is the total hybridization as before. The dimensionless $G_0 = 4\Gamma_s\Gamma_d/(\Gamma_s + \Gamma_d)^2$ embodies simply the relative coupling to source and drain

leads, such that for $\Gamma_s = \Gamma_d$, $G_0 = 1$ is maximal, while in the extreme asymmetric limit $\Gamma_s \gg \Gamma_d$ (where the drain acts as a weak tunneling probe), $G_0 \sim 4\Gamma_d/\Gamma_s \ll 1$.

For $T = 0$, Eq. (44) reduces simply to

$$G_c^0 = \frac{2e^2}{h} G_0 \pi \Gamma D_1(\omega = 0), \quad (45)$$

and Eq. (42) then gives a universal zero-bias conductance $G_c^0/G_0 = e^2/h$ at $T = 0$, obtained for any value of the gate voltage $V_g \propto \epsilon$. This result is thus consistent with that known for related models in the singly occupied Kondo limit, which demonstrate 2CK behavior (see, e.g., Refs. 15–18,24,42,45). For finite T , the Fermi level value of the spectrum has the same low- T/T_K^{2CK} dependence⁴⁵ as the $T = 0$ spectrum does of ω/T_K^{2CK} [Eq. (42)], viz., $\pi \Gamma D_1(\omega = 0; T) \sim \frac{1}{2}[1 - b'(T/T_K^{2CK})^{1/2}]$. Combined with Eq. (42), Eq. (44) is then readily shown⁴⁵ to yield $G_c(T)/G_0 \sim \frac{e^2}{h}[1 - \gamma(T/T_K^{2CK})^{1/2}]$, with $\gamma = b' + b\sqrt{\pi}\eta(\frac{1}{2})$ and $\sqrt{\pi}\eta(\frac{1}{2}) \simeq 1.07$, which T dependence is also known to arise for the single-spin 2CK model.^{13,16,17,70}

Calculating the conductance at finite bias is of course a different matter, and an exact (or even numerically exact) treatment of the underlying nonequilibrium physics is a formidable open problem. Here we merely make the simplifying approximation that the self-energy does not depend explicitly on the bias voltage,⁷⁹ which leads to

$$G_c \simeq \frac{e^2}{h} G_0 \int_{-\infty}^{\infty} d\omega \left(-\frac{\partial f_s(\omega)}{\partial \omega} - \frac{\partial f_d(\omega)}{\partial \omega} \right) \pi \Gamma D_1(\omega), \quad (46)$$

where $f_\gamma(\omega) = [e^{(\omega - \mu_\gamma)/T} + 1]^{-1}$ is the Fermi function for the $\gamma = s/d$ lead. While this approximation is exact both for $V_{sd} = 0$ and for all V_{sd} in the extreme asymmetric limit $\Gamma_s \gg \Gamma_d$ (Ref. 22) (conductance measured with a “perfect STM”), in the standard case relevant to semiconductor quantum dot devices, the leads are more symmetrically coupled. Here we

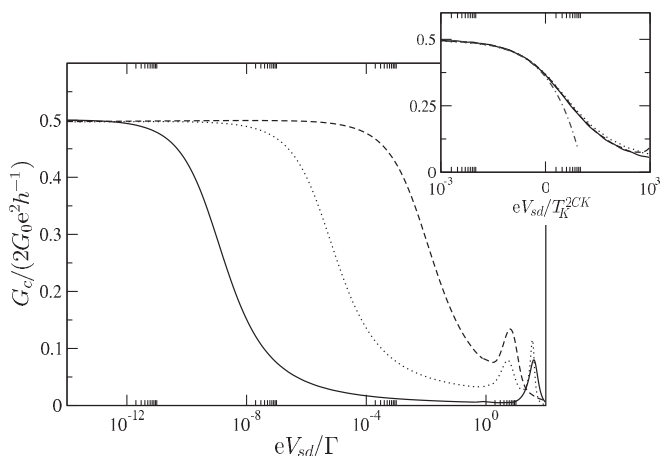


FIG. 17. Conductance $G_c/(2G_0e^2h^{-1})$ vs eV_{sd}/Γ for systems with the same parameters as Figs. 14 and 16. Inset: scaling collapse to a universal curve with asymptotic $eV_{sd} \ll T_K^{2CK}$ behavior $G_c(V_{sd}) = G_0e^2h^{-1}[1 - b(eV_{sd}/T_K^{2CK})^{1/2}]$ (dot-dashed line).

consider a symmetric voltage split between the leads, $\mu_{s/d} = \pm \frac{1}{2}eV_{sd}$, for which Eq. (46) yields

$$G_c(V_{sd}) \simeq \frac{e^2}{h} G_0 \pi \Gamma \left[D_1 \left(\omega = \frac{1}{2}eV_{sd} \right) + D_1 \left(\omega = -\frac{1}{2}eV_{sd} \right) \right] \quad (47)$$

for $T = 0$. This approximation thus allows us to work with single-particle spectra determined at equilibrium, obtained from a two-lead NRG calculation^{59–61,67} as before.

Figure 17 shows the resultant differential conductance $G_c/(2G_0e^2h^{-1})$ versus eV_{sd}/Γ , calculated using Eq. (47), for the same $\mathcal{N} = 3, 4, 5$ systems as in Figs. 14 and 16. Since the conductance comprises a symmetrized combination of the total dot spectrum, similar features to that in Fig. 16 are naturally observed. Peaks at high bias originate from the Hubbard satellites and correspond to simple single-electron sequential tunneling processes. Importantly, the Kondo resonance also of course shows up, with the zero-bias value of $G_c^0/G_0 = e^2/h$ arising for $eV_{sd} \ll T_K^{2CK}$ in each case. Universal scaling of the conductance in terms of eV_{sd}/T_K^{2CK} is also shown in the inset, demonstrating in particular the $eV_{sd} \ll T_K^{2CK}$ asymptotic form

$$G_c(V_{sd}) \underset{\frac{eV_{sd}}{T_K^{2CK}} \ll 1}{\sim} \frac{e^2}{h} G_0 [1 - b(eV_{sd}/T_K^{2CK})^{1/2}], \quad (48)$$

which behavior is likewise known^{15,16,18} in the NFL regime of the 2CK device constructed in Ref. 18.

D. Phase shifts and the S matrix

We now consider the leading low- ω behavior of the single-particle scattering S matrix, $S(\omega) = e^{2i\delta(\omega)}$, and associated phase shift $\delta(\omega) = \delta_R(\omega) + i\delta_I(\omega)$. The S matrix is given by⁶⁵

$$S(\omega) = 1 - 2i\Gamma G_1(\omega), \quad (49a)$$

with $\Gamma G_1(\omega)$ related to the $t_L(\omega)$ matrix by

$$\pi \rho_T t_L(\omega) = \Gamma G_1(\omega) \quad (49b)$$

such that (as in Sec. III C) $-\pi \rho_T \text{Im} t_L(\omega) = \pi \Gamma D_1(\omega)$. It follows from Eq. (49a) that

$$\pi \Gamma D_1(\omega) = \frac{1}{2} \{1 - e^{-2\delta_I(\omega)} \cos[2\delta_R(\omega)]\}, \quad (50)$$

leading in particular to the limiting behavior

$$\pi \Gamma D_1(\omega) = \begin{cases} \sin^2[\delta_R(\omega)], & \delta_I(\omega) \rightarrow 0, \\ \frac{1}{2}, & \delta_I(\omega) \rightarrow \infty. \end{cases} \quad (51)$$

To obtain $S(\omega)$, it is convenient to express the propagator as $G_1(\omega) = [A(\omega) + iB(\omega)]^{-1}$, where

$$A(\omega) = \omega - \epsilon - \Sigma_1^R(\omega), \quad B(\omega) = \Gamma + \Sigma_1^I(\omega) \quad (52)$$

such that $A(0) = -\epsilon^*$ and $B(0) = \Gamma^*$ by Eq. (40) [and for simplicity we take here the wide-band limit for the lead density of states, $\Gamma(\omega) = -i\Gamma$, which does not affect any of the following results]. From Eq. (49a) it follows that

$$e^{2i\delta(\omega)} = \frac{A(\omega) - iB'(\omega)}{A(\omega) + iB(\omega)}, \quad (53)$$

where

$$B'(\omega) = \Gamma - \Sigma_1^I(\omega). \quad (54)$$

First consider the familiar situation that would arise if the system were a regular Fermi liquid, for which $\Sigma_1^f(\omega = 0) = 0$. In this case, $B(0) = B'(0)$, and Eq. (53) yields $\delta(0) = \arg[G_1(0)]$. The S matrix is then unitary at the Fermi level, $|S(0)|^2 = 1$, and, since $\delta_I(0) = 0$, the Fermi level spectrum follows from Eq. (51) as $\pi\Gamma D_1(0) = \sin^2[\delta_R(0)]$.

The situation is of course quite different for the present problem. The low-frequency behavior of the self-energy is given by Eqs. (43), and from which Eqs. (52)–(54) yield

$$e^{2i\delta(\omega)} \sim b \left(\frac{|\omega|}{T_K^{2\text{CK}}} \right)^{\frac{1}{2}} [1 - i \operatorname{sgn}(\omega)] \quad (55)$$

as the leading asymptotic form for $|\omega|/T_K^{2\text{CK}} \rightarrow 0$, i.e.,

$$\delta_R(\omega) \sim \frac{1}{2} \arctan[-\operatorname{sgn}(\omega)], \quad (56a)$$

$$e^{-2\delta_I(\omega)} \sim \sqrt{2} b \left(\frac{|\omega|}{T_K^{2\text{CK}}} \right)^{\frac{1}{2}}. \quad (56b)$$

In evident contrast to a FL, the imaginary part of the phase shift thus diverges logarithmically as $\omega \rightarrow 0$,

$$\delta_I(\omega) \sim -\frac{1}{4} \ln(|\omega|/T_K^{2\text{CK}}), \quad (57)$$

the divergence itself reflecting [see Eq. (51)] the pinning of the Fermi level spectrum to a half-unitary value (Sec. III C). As a consequence, the S matrix vanishes at the Fermi level, $S(0) = 0$, as is known for the single spin- $\frac{1}{2}$ 2CK model.^{80–82} This does not of course mean that an electron sent in to scatter off the dot is “absorbed” (the conductance being generically nonzero), but rather that electrons scatter completely into collective excitations, characteristic of the NFL state.^{80,82}

Notice also from Eq. (56a) that the real part of the phase shift is discontinuous across the Fermi level, and that $\delta_R(\omega = 0\pm) \neq \arg[G_1(0)]$ (again in contrast to a FL). $\cos[2\delta_R(0)] = 1/\sqrt{2}$ is, however, continuous across $\omega = 0$, and, combined with Eq. (56b), Eq. (50) recovers precisely Eq. (42) for the low- ω asymptotics of $\pi\Gamma D_1(\omega)$.

E. Friedel-Luttinger sum rule

We now consider further implications of the pinning of the $T = 0$ Fermi level spectrum, $\pi\Gamma D_1(0) = \frac{1}{2}$, regardless of bare model parameters and even when the dot occupancies change drastically on varying the bare level energy ϵ . In particular, we obtain an analog of the Friedel sum rule^{19,65}—a Friedel-Luttinger sum rule⁶²—relating the Fermi level spectrum to the “excess” charge induced by addition of the impurity chain,¹⁹ via the Luttinger integral.^{63,64}

To this end, consider first the excess charge n_{imp} , defined as the difference in charge of the entire system with and without the trimeric impurity chain,¹⁹ and also n'_{imp} , defined correspondingly but with only the two terminal dots (“1” and “3”) of the chain removed. Since impurity “2” is a strict spin, it follows trivially that $n_{\text{imp}} = n'_{\text{imp}} + 1$. Using, e.g., equation of motion methods,^{19,66} it is readily shown that

$$n'_{\text{imp}} = -\frac{4}{\pi} \operatorname{Im} \int_{-\infty}^0 d\omega G_1(\omega) \left[1 - \frac{\partial \Gamma(\omega)}{\partial \omega} \right] \quad (58)$$

(noting that sites “1” and “3” are equivalent by symmetry). In practice, as expected physically, n'_{imp} differs negligibly from

the charge $2\langle \hat{n}_1 \rangle$ on the terminal dots, to which it reduces precisely in the wide flat-band limit where $\Gamma(\omega) = -i\Gamma$ is constant.

Note next that Eq. (41) can be written as

$$\pi\Gamma D_1(\omega = 0) = (\Gamma/\Gamma^*) \sin^2(\theta) \quad (59)$$

with $\theta = \arctan(\Gamma^*/\epsilon^*)$ ($\equiv \arg[G_1(0)]$). Equivalently, using $\arg[G_1(\omega = -\infty)] = 0$,

$$\theta = \operatorname{Im} \int_{-\infty}^0 d\omega \frac{\partial}{\partial \omega} \ln G_1(\omega). \quad (60)$$

But from the definition of the propagator, $G_1(\omega) = [\omega^+ - \epsilon - \Gamma(\omega) - \Sigma_1(\omega)]^{-1}$, it follows that

$$\frac{\partial}{\partial \omega} \ln G_1(\omega) = -G_1(\omega) \left[1 - \frac{\partial \Gamma(\omega)}{\partial \omega} \right] + G_1(\omega) \frac{\partial \Sigma_1(\omega)}{\partial \omega}. \quad (61)$$

The Friedel-Luttinger sum rule then follows directly from Eq. (60) as

$$\theta = \frac{\pi}{4} n'_{\text{imp}} + I_L, \quad (62)$$

where the Luttinger integral^{63,64}

$$I_L = \operatorname{Im} \int_{-\infty}^0 d\omega G_1(\omega) \frac{\partial \Sigma_1(\omega)}{\partial \omega} \quad (63)$$

involves integration over all energy scales.

Again consider briefly the situation that would arise if the system were a normal FL. In this case, the Luttinger integral vanishes^{63,64} regardless of bare model parameters, and $\theta \equiv \delta_R(0)$ (as in Sec. III D). Equation (62) then reduces to a Friedel sum rule,^{19,65} relating the static phase shift to the excess charge.

The present problem is not of course a Fermi liquid, and I_L does not vanish. The single-particle spectrum is, however, ubiquitously pinned at $\pi\Gamma D_1(\omega = 0) = \frac{1}{2}$ (i.e., $\Gamma^* = 2\Gamma$ and $\epsilon^* = 0$), from which $\theta = \pi/2$ regardless of bare parameters.

Equation (62) in this case thus becomes a sum rule relating the Luttinger integral to the excess charge:

$$I_L = \frac{\pi}{4} (2 - n'_{\text{imp}}) = \frac{\pi}{4} (3 - n_{\text{imp}}). \quad (64)$$

Under the particle-hole transformation Eq. (29), it is easily shown that $n'_{\text{imp}} \rightarrow 4 - n'_{\text{imp}}$ (or equivalently $n_{\text{imp}} \rightarrow 6 - n_{\text{imp}}$). Hence $I_L \rightarrow -I_L$ under the transformation, and in particular it vanishes at the particle-hole symmetric point $\epsilon = -U/2$, where $n_{\text{imp}} = 3$ identically.

The behavior of n_{imp} as, e.g., the level energy ϵ is varied is naturally a smoothed and continuous version of the Coulomb-blockade staircase arising in the atomic limit (where on varying ϵ the total number of electrons in the free chain, \mathcal{N} , jumps discontinuously between integer values characteristic of each CB valley). I_L itself will thus reflect that variation, and sufficiently deep in each CB valley, where $n_{\text{imp}} (\simeq \mathcal{N})$ is close to integral, each regime may be loosely associated with its own value of I_L .

The above discussion is exemplified clearly by Fig. 18, where the Luttinger integral I_L/π is shown versus the level energy $\epsilon/\pi\Gamma$ for systems with common $U/\pi\Gamma = 10$ and $\rho J = 0.075$. The points correspond to direct calculation of I_L via Eq. (63), using the full Green function and self-energy from NRG. The line is simply Eq. (64), using n_{imp} as determined

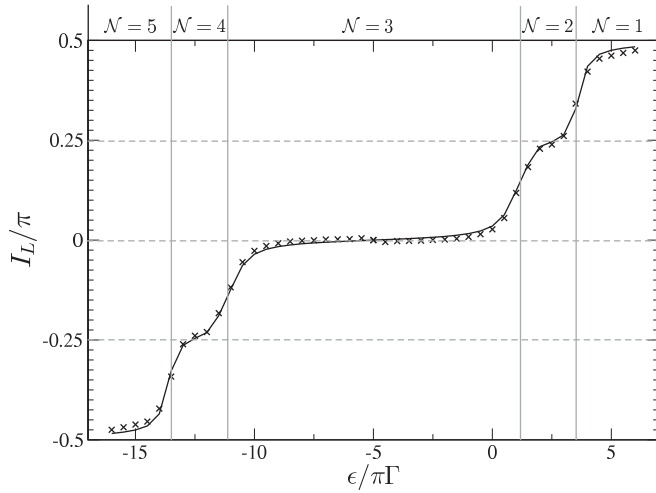


FIG. 18. Luttinger integral I_L/π vs level energy $\epsilon/\pi\Gamma$ for systems with $\rho J = 0.075$, $U/\pi\Gamma = 10$, and $\Gamma/D = 10^{-2}$. Direct calculation via Eq. (63) shown as points, compared with Eq. (64) (line) using n_{imp} determined from a standard thermodynamic NRG calculation.

from a standard thermodynamic NRG calculation.⁵⁸ The agreement is excellent over the wide range of electron fillings shown, the overall form of the curve reflecting the smoothed CB staircase as anticipated above.

Our focus has been the $N_c = 3$ trimer, but for longer (odd) chains one naturally expects the same 2CK physics to occur on low-energy scales. We have indeed confirmed this explicitly by NRG for the $N_c = 5$ case. In particular, the single-particle spectrum of dot “1” at the Fermi level is again always pinned to half-unity, $\pi\Gamma D_1(\omega = 0) = \frac{1}{2}$ (from which the zero-bias conductance through a terminal dot remains $G_c/G_0 = e^2/h$). The result $\theta = \pi/2$ thus holds generally, as does the Friedel-Luttinger sum rule Eq. (62), with n'_{imp} now related to the total excess charge by $n_{\text{imp}} = n'_{\text{imp}} + (N_c - 2)$, and as a consequence, the general result for the Luttinger integral for odd chains follows:

$$I_L = \frac{\pi}{4}(2 - n'_{\text{imp}}) = \frac{\pi}{4}(N_c - n_{\text{imp}}). \quad (65)$$

IV. CONCLUDING REMARKS: REAL QUANTUM DOT SYSTEMS

The exchange-coupled impurity chains studied in this paper may be considered as approximate low-energy models of quantum dot devices. In real systems, however, the dots are mutually tunnel-coupled rather than pure exchange-coupled; the 2CK fixed point is rendered unstable by the interlead charge transfer that results, and the system crosses over to FL behavior on a low-energy scale $T \lesssim T_{\text{FL}}$. Experimental access to 2CK physics must thus contend with both channel anisotropy (as studied in Sec. II) and charge-transfer terms. On the level of a toy model calculation, we now consider briefly the generic behavior arising when the latter perturbation is included, considering explicitly the L/R mirror symmetric case (although the analysis is readily extended to include explicit channel anisotropy).

To motivate this, recall that a single ($N_c = 1$) one-level quantum dot tunnel-coupled to two metallic leads does not of course exhibit 2CK physics.^{20–22} This follows from the Anderson Hamiltonian itself, $H_{\text{And}} = H_{\text{dot}} + \sum_{\alpha=L/R}[H_L^\alpha + H_{\text{hyb}}^\alpha]$, where $H_{\text{dot}} = \epsilon(\hat{n}_{d\uparrow} + \hat{n}_{d\downarrow}) + U\hat{n}_{d\uparrow}\hat{n}_{d\downarrow}$, $H_L^\alpha = \sum_{\mathbf{k},\sigma} \epsilon_{\mathbf{k}} a_{\alpha\mathbf{k}\sigma}^\dagger a_{\alpha\mathbf{k}\sigma}$, and $H_{\text{hyb}}^\alpha = V \sum_{\mathbf{k},\sigma} (a_{\alpha\mathbf{k}\sigma}^\dagger d_\sigma + \text{H.c.})$. Transforming canonically to even (e) and odd (o) lead orbitals,

$$a_{e\mathbf{k}\sigma} = \frac{1}{\sqrt{2}}(a_{L\mathbf{k}\sigma} + a_{R\mathbf{k}\sigma}), \quad (66)$$

$$a_{o\mathbf{k}\sigma} = \frac{1}{\sqrt{2}}(a_{L\mathbf{k}\sigma} - a_{R\mathbf{k}\sigma}),$$

H_{And} is equivalent to $H_{\text{And}} = H_{\text{dot}} + H_L^e + \sqrt{2}H_{\text{hyb}}^e$, in which the dot couples solely to the e -lead, exhibiting as such single-channel physics only.

In the singly occupied dot regime, a low-energy spin- $\frac{1}{2}$ Kondo model follows from a SW transformation^{19,77} of H_{And} , leading simply to $H_{\text{SW}} = H_L^L + H_L^R + H_K$ with

$$H_K = J_K \hat{\mathbf{S}} \cdot (\hat{\mathbf{s}}_{L0} + \hat{\mathbf{s}}_{R0}) + J_{LR} \hat{\mathbf{S}} \cdot \hat{\mathbf{s}}_{LR0} \quad (67)$$

(potential scattering is ignored), where $\hat{\mathbf{s}}_{\alpha 0}$ is given by Eq. (2) and $\hat{\mathbf{s}}_{LR0}$ is defined as

$$\hat{\mathbf{s}}_{LR0} = \sum_{\sigma,\sigma',\alpha} f_{\alpha 0\sigma}^\dagger \sigma_{\sigma\sigma'} f_{\alpha 0\sigma'} \quad (68)$$

with $\bar{\alpha} = R, L$ for $\alpha = L, R$. Equation (67) consists formally of a symmetric 2CK model—the first term—together with a term $\hat{\mathbf{S}} \cdot \hat{\mathbf{s}}_{LR0}$ that transfers (cotunnels) charge between the leads. In fact, applying the transformation Eq. (66) yields $H_{\text{SW}} = H_L^e + H_L^o + H_K$ with

$$H_K = J_K \hat{\mathbf{S}} \cdot (\hat{\mathbf{s}}_{e0} + \hat{\mathbf{s}}_{o0}) + J_{LR} \hat{\mathbf{S}} \cdot (\hat{\mathbf{s}}_{e0} - \hat{\mathbf{s}}_{o0}), \quad (69)$$

where $\hat{\mathbf{s}}_{e0}$ and $\hat{\mathbf{s}}_{o0}$ are e/o lead spin densities, a model that is generically of channel-asymmetric 2CK form. But for the single-dot Anderson model itself, the couplings are necessarily equal, $J_{LR} = J_K$. In this case, the dot is exchange-coupled solely to the even lead, and Eq. (69) reduces as it must to a single-channel Kondo model with Kondo coupling $2J_K$.

In systems comprising several tunnel-coupled quantum dots, however, cotunneling charge-transfer can be effectively suppressed,²⁴ with $J_{LR} \ll J_K$ expected for longer chains (a simple estimate yielding $J_{LR}/J_K \sim [t/U]^{N_c-1}$ with t the inter-dot tunnel coupling). Here we simply regard Eq. (67), with $J_{LR} \neq J_K$, as an effective toy model to mimic such effects in odd- N_c dot chains (with $\hat{\mathbf{S}}$ representing the lowest chain doublet). From Eq. (69) it is clear that the resultant low-energy or low-temperature physics is then that of the channel-asymmetric 2CK model.^{1–3,10,14} The 2CK FP is thus rendered unstable by the perturbation J_{LR} , any nascent 2CK state forming at $T_K^{2\text{CK}}$ being destroyed below the FL crossover scale T_{FL} , although inclusion of the J_{LR} term should not obscure the 2CK physics for $T \gg T_{\text{FL}}$, provided J_{LR} itself is sufficiently small. Note also that any *direct* interlead tunneling terms of the type $\sum_{\mathbf{k},\mathbf{k}'} (a_{L\mathbf{k}\sigma}^\dagger a_{R\mathbf{k}'\sigma} + \text{H.c.})$ —as opposed to cotunneling, which intrinsically proceeds via the dot spin—are equivalent [through the transformation Eq. (66)] to simple

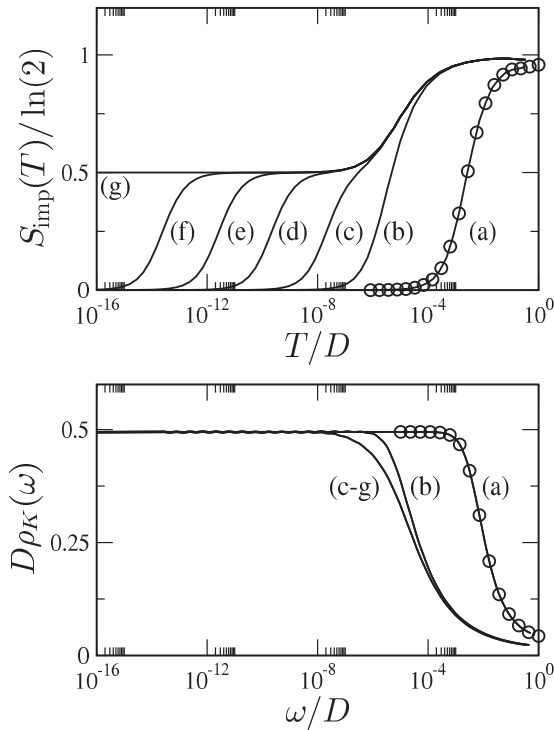


FIG. 19. Upper panel: entropy $S_{\text{imp}}(T)$ vs T/D for a single-spin 2CK model with explicit left-right lead charge transfer [see Eq. (67)]. Shown for fixed $\rho J_K = 10^{-1}$, varying $\rho J_{LR} = 10^{-1}, 10^{-2}, 10^{-3}, 10^{-4}, 10^{-5}, 10^{-6}$ [lines (a)–(f)], successively approaching the pure 2CK limit with $\rho J_{LR} = 0$, line (g). Lower panel: $T = 0$ spectra $D\rho_K(\omega)$ vs ω/D for the same systems. $S_{\text{imp}}^{\text{1CK}}(T)$ and $\frac{1}{2}D\rho_K^{\text{1CK}}(\omega)$ for a 1CK model with $\rho J_K = 0.2$ (circles) are also shown for comparison.

potential scattering in the even and odd channels. This does not destabilize the 2CK FP,¹¹ which is why we do not include such terms here.

The above scenario is explored in Fig. 19, where NRG results for Eq. (67) are shown. We fix $\rho J_K = 10^{-1}$ and vary the cotunneling term $\rho J_{LR} = 10^{-1}, 10^{-2}, 10^{-3}, 10^{-4}, 10^{-5}$ and 10^{-6} [lines (a)–(f)], approaching the pure 2CK limit $J_{LR} = 0$ [line (g)]. The top panel shows the entropy $S_{\text{imp}}(T)/\ln(2)$ versus T/D , from which the behavior associated with the channel-asymmetric 2CK model^{1–3,10,14} is seen to arise, as expected from Eq. (69). In the extreme case $J_K = J_{LR}$ [line (a)], the odd channel is completely decoupled, no 2CK physics occurs, and the behavior is that of a single-channel Kondo model (circles), the impurity entropy being completely quenched below $T \sim T_K^{\text{1CK}}$ [cf. Eq. (14)]. For smaller $J_{LR} \lesssim T_K^{\text{1CK}}$, however, the 2CK scale T_K^{2CK} emerges [cf. Eq. (8)], below which temperature a characteristic $S_{\text{imp}} = \frac{1}{2} \ln(2)$ plateau occurs [lines (d)–(g)]. Flow to the FL FP below $T \sim T_{\text{FL}}$, for all systems with $J_{LR} \neq 0$, is then manifest in the

final drop to $S_{\text{imp}} = 0$, the FL crossover scale T_{FL} being found to vanish as

$$T_{\text{FL}} \stackrel{J_{LR} \rightarrow 0^\pm}{\sim} \mathcal{A} |J_{LR}|^\nu, \quad \nu = 2 \quad (70)$$

with exponent $\nu = 2$, just as expected from mapping to the channel-asymmetric 2CK model, Eq. (69).

We turn now to the $T = 0$ spectra $D\rho_K(\omega) \equiv D\rho_{K,\alpha}(\omega) = -\pi\rho_T \text{Im}[t_\alpha(\omega)]$ for lead $\alpha = L$ or R (the two being equivalent by mirror symmetry), shown in the lower panel of Fig. 19. The spectral behavior is rather different from what might naively be expected from the entropy, since no low-energy T_{FL} scale is apparent (compare, e.g., to the channel-asymmetric 2CK models studied in Fig. 7). This, however, reflects the fact that the model Eq. (67) is channel-asymmetric 2CK in the e/o basis [Eq. (69)], rather than the L/R basis, and is readily understood using the transformation Eq. (66), from which one obtains $D\rho_{K,\alpha}(\omega) = \frac{1}{2}[D\rho_{K,e}(\omega) + D\rho_{K,o}(\omega)]$ in terms of the spectra for e/o channels. For $J_K = J_{LR}$ [line (a)], the odd channel is decoupled in Eq. (69), so $D\rho_{K,\alpha}(\omega) = \frac{1}{2}D\rho_{K,e}(\omega) \equiv \frac{1}{2}D\rho_K^{\text{1CK}}(\omega)$, where $D\rho_K^{\text{1CK}}(\omega)$ is the spectrum for a 1CK model with Kondo coupling $2J_K$ [as confirmed explicitly (circles) in the lower panel of Fig. 19].

However, for lines (c)–(f) (corresponding to $J_{LR} \ll T_K^{\text{1CK}}$), the spectra are indistinguishable from the pure 2CK spectrum, line (g), over the *entire* range of frequencies. For $T_{\text{FL}} \ll |\omega| \ll T_K^{\text{2CK}}$, RG flow in the vicinity of the 2CK FP naturally results in the universal behavior $D\rho_{K,e}(\omega) = D\rho_{K,o}(\omega) = \frac{1}{2}[1 - b(|\omega|/T_K^{\text{2CK}})^{1/2}]$, as expected for a 2CK model with small even-odd channel asymmetry (see Fig. 7). Consequently, $D\rho_K(\omega)$ shows the same behavior. For $|\omega| \ll T_{\text{FL}}$, by contrast, the spectrum for the more strongly coupled e -channel has the asymptotic form $D\rho_{K,e}(\omega) = 1 - d(|\omega|/T_{\text{FL}})^2$, while the weakly coupled o -channel is described by $D\rho_{K,o}(\omega) = d(|\omega|/T_{\text{FL}})^2$ (see Fig. 7 and discussion thereof). Indeed, we found in Sec. II A that the *entire* universal crossover to the Fermi liquid FP for the strongly coupled lead is related to that of the weakly coupled lead by $D\rho_{K,e}(\omega) = 1 - D\rho_{K,o}(\omega)$. Thus, $D\rho_K(\omega) = \frac{1}{2}$ arises for *all* $|\omega| \ll T_K^{\text{2CK}}$, as indeed found. As such, the spectrum $D\rho_K(\omega)$ is effectively “blind” to the Fermi liquid crossover induced by small finite J_{LR} : the 2CK FP appears to be stable on the lowest energy scales—although from, e.g., the entropy, we know that this is not the case. Ironically, then, experiments that probe the t matrix (such as measurement of the zero-bias conductance across dot “1”) will always appear to yield 2CK physics, provided $J_{LR} \lesssim T_K^{\text{1CK}}$.

ACKNOWLEDGMENTS

Helpful discussions with M. Galpin and E. Sela are gratefully acknowledged. This work was funded in part by EPSRC (UK) under Grant No. EP/D050952/1. A.K.M. also thanks the DFG for financial support through SFB 608 and FOR 960.

¹P. Nozières and A. Blandin, *J. Phys. (Paris)* **41**, 193 (1980).

²P. D. Sacramento and P. Schlottmann, *Phys. Lett. A* **142**, 245 (1989).

³N. Andrei and A. Jerez, *Phys. Rev. Lett.* **74**, 4507 (1995).

⁴N. Andrei and C. Destri, *Phys. Rev. Lett.* **52**, 364 (1984).

⁵A. M. Tselvelick and P. B. Wiegmann, *Z. Phys. B* **54**, 201 (1984).

- ⁶G. Zaránd, T. Costi, A. Jerez, and N. Andrei, *Phys. Rev. B* **65**, 134416 (2002).
- ⁷D. M. Cragg and P. Lloyd, *J. Phys. C* **12**, 3301 (1979).
- ⁸D. M. Cragg, P. Lloyd, and P. Nozières, *J. Phys. C* **13**, 803 (1980).
- ⁹H.-B. Pang and D. L. Cox, *Phys. Rev. B* **44**, 9454 (1991).
- ¹⁰I. Affleck, A. W. W. Ludwig, H.-B. Pang, and D. L. Cox, *Phys. Rev. B* **45**, 7918 (1992).
- ¹¹I. Affleck and A. W. W. Ludwig, *Nucl. Phys. B* **360**, 641 (1990).
- ¹²A. W. W. Ludwig and I. Affleck, *Phys. Rev. Lett.* **67**, 3160 (1991).
- ¹³I. Affleck and A. W. W. Ludwig, *Phys. Rev. B* **48**, 7297 (1993).
- ¹⁴D. L. Cox and A. Zawadowski, *Adv. Phys.* **47**, 599 (1998).
- ¹⁵Y. Oreg and D. Goldhaber-Gordon, *Phys. Rev. Lett.* **90**, 136602 (2003).
- ¹⁶M. Pustilnik, L. Borda, L. I. Glazman, and J. von Delft, *Phys. Rev. B* **69**, 115316 (2004).
- ¹⁷A. I. Tóth, L. Borda, J. von Delft, and G. Zaránd, *Phys. Rev. B* **76**, 155318 (2007).
- ¹⁸R. M. Potok, I. G. H. Shtrikman, Y. Oreg, and D. Goldhaber-Gordon, *Nature (London)* **446**, 167 (2007).
- ¹⁹A. C. Hewson, *The Kondo Problem to Heavy Fermions* (Cambridge University Press, Cambridge, 1993).
- ²⁰D. Goldhaber-Gordon, H. Shtrikman, D. Mahalu, D. Abusch-Magder, U. Meirav, and M. A. Kastner, *Nature (London)* **391**, 156 (1998).
- ²¹S. M. Cronenwett, T. H. Oosterkamp, and L. P. Kouwenhoven, *Science* **281**, 540 (1998).
- ²²M. Pustilnik and L. I. Glazman, *J. Phys. Condens. Matter* **16**, R513 (2004).
- ²³L. P. Kouwenhoven, C. M. Marcus, P. L. McEuen, S. Tarucha, R. M. Westervelt, and N. S. Wingreen, in *Mesoscopic Electron Transport*, edited by L. L. Sohn, L. P. Kouwenhoven, and G. Schön (Kluwer, Dordrecht, 1997).
- ²⁴G. Zaránd, C.-H. Chung, P. Simon, and M. Vojta, *Phys. Rev. Lett.* **97**, 166802 (2006).
- ²⁵B. A. Jones, C. M. Varma, and J. W. Wilkins, *Phys. Rev. Lett.* **61**, 125 (1988).
- ²⁶B. A. Jones and C. M. Varma, *Phys. Rev. B* **40**, 324 (1989).
- ²⁷E. Sela and I. Affleck, *Phys. Rev. Lett.* **102**, 047201 (2009).
- ²⁸E. Sela and I. Affleck, *Phys. Rev. Lett.* **103**, 087204 (2009).
- ²⁹M. Vojta, R. Bulla, and W. Hofstetter, *Phys. Rev. B* **65**, 140405(R) (2002).
- ³⁰M. Garst, S. Kehrein, T. Pruschke, A. Rosch, and M. Vojta, *Phys. Rev. B* **69**, 214413 (2004).
- ³¹M. R. Galpin, D. E. Logan, and H. R. Krishnamurthy, *Phys. Rev. Lett.* **94**, 186406 (2005).
- ³²A. K. Mitchell, M. R. Galpin, and D. E. Logan, *Europhys. Lett.* **76**, 95 (2006).
- ³³D. Boese, W. Hofstetter, and H. Schoeller, *Phys. Rev. B* **66**, 125315 (2002).
- ³⁴P. S. Cornaglia and D. R. Grempel, *Phys. Rev. B* **71**, 075305 (2005).
- ³⁵R. Žitko and J. Bonča, *J. Phys. Condens. Matter* **19**, 255205 (2007).
- ³⁶R. Žitko, *Phys. Rev. B* **81**, 115316 (2010).
- ³⁷A. Oguri and A. C. Hewson, *J. Phys. Soc. Jpn.* **74**, 2554 (2005).
- ³⁸T. Kuzmenko, K. Kikoin, and Y. Avishai, *Phys. Rev. B* **73**, 235310 (2006).
- ³⁹R. Žitko, J. Bonča, A. Ramšak, and T. Rejec, *Phys. Rev. B* **73**, 153307 (2006).
- ⁴⁰A. K. Mitchell, T. F. Jarrold, and D. E. Logan, *Phys. Rev. B* **79**, 085124 (2009).
- ⁴¹T. Numata, Y. Nisikawa, A. Oguri, and A. C. Hewson, *Phys. Rev. B* **80**, 155330 (2009).
- ⁴²R. Žitko and J. Bonča, *Phys. Rev. Lett.* **98**, 047203 (2007).
- ⁴³R. Žitko and J. Bonča, *Phys. Rev. B* **77**, 245112 (2008).
- ⁴⁴E. Vernek, C. A. Büsser, G. B. Martins, E. V. Anda, N. Sandler, and S. E. Ulloa, *Phys. Rev. B* **80**, 035119 (2009).
- ⁴⁵A. K. Mitchell and D. E. Logan, *Phys. Rev. B* **81**, 075126 (2010).
- ⁴⁶M. Ferrero, L. D. Leo, P. Lecheminant, and M. Fabrizio, *J. Phys. Condens. Matter* **19**, 433201 (2007).
- ⁴⁷R. H. Blick, R. J. Haug, J. Weis, D. Pfannkuche, K. v. Klitzing, and K. Eberl, *Phys. Rev. B* **53**, 7899 (1996).
- ⁴⁸W. G. van der Wiel, S. D. Franceschi, T. Fukisawa, J. M. Elzerman, S. Tarucha, and L. P. Kouwenhoven, *Science* **289**, 2105 (2000).
- ⁴⁹H. Jeong, A. M. Chang, and M. R. Melloch, *Science* **293**, 2221 (2001).
- ⁵⁰A. Vidan, R. Westervelt, M. Stopa, M. Hanson, and A. Gossard, *J. Supercond. Incorp. Novel Magn.* **18**, 223 (2005).
- ⁵¹D. Schröer, A. D. Greentree, L. Gaudreau, K. Eberl, L. C. L. Hollenberg, J. P. Kotthaus, and S. Ludwig, *Phys. Rev. B* **76**, 075306 (2007).
- ⁵²M. C. Rogge and R. J. Haug, *Phys. Rev. B* **77**, 193306 (2008).
- ⁵³K. Grove-Rasmussen, H. I. Jørgensen, T. Hayashi, P. E. Lindelof, and T. Fujisawa, *Nano Lett.* **8**, 1055 (2008).
- ⁵⁴N. Roch, S. Florens, V. Bouchiat, W. Wernsdorfer, and F. Balestro, *Nature (London)* **453**, 633 (2008).
- ⁵⁵L. Gaudreau, A. S. Sachrajda, S. Studenikin, A. Kam, F. Delgado, Y. P. Shim, M. Korkusinski, and P. Hawrylak, *Phys. Rev. B* **80**, 075415 (2009).
- ⁵⁶G. Granger, L. Gaudreau, A. Kam, M. Pioro-Ladrière, S. A. Studenikin, Z. R. Wasilewski, P. Zawadzki, and A. S. Sachrajda, *Phys. Rev. B* **82**, 075304 (2010).
- ⁵⁷K. G. Wilson, *Rev. Mod. Phys.* **47**, 773 (1975).
- ⁵⁸H. R. Krishna-murthy, J. W. Wilkins, and K. G. Wilson, *Phys. Rev. B* **21**, 1003 (1980); **21**, 1044 (1980).
- ⁵⁹R. Bulla, T. Costi, and T. Pruschke, *Rev. Mod. Phys.* **80**, 395 (2008).
- ⁶⁰R. Peters, T. Pruschke, and F. B. Anders, *Phys. Rev. B* **74**, 245114 (2006).
- ⁶¹A. Weichselbaum and J. von Delft, *Phys. Rev. Lett.* **99**, 076402 (2007).
- ⁶²D. E. Logan, C. J. Wright, and M. R. Galpin, *Phys. Rev. B* **80**, 125117 (2009).
- ⁶³J. M. Luttinger, *Phys. Rev.* **119**, 1153 (1960).
- ⁶⁴J. M. Luttinger and J. C. Ward, *Phys. Rev.* **118**, 1417 (1960).
- ⁶⁵D. C. Langreth, *Phys. Rev.* **150**, 1516 (1966).
- ⁶⁶D. N. Zubarev, *Sov. Phys. Usp.* **3**, 320 (1960).
- ⁶⁷R. Bulla, A. C. Hewson, and T. Pruschke, *J. Phys. Condens. Matter* **10**, 8365 (1998).
- ⁶⁸H. Johannesson, C. J. Bolech, and N. Andrei, *Phys. Rev. B* **71**, 195107 (2005).
- ⁶⁹S. C. Bradley, R. Bulla, A. C. Hewson, and G.-M. Zhang, *Eur. Phys. J. B* **11**, 535 (1999).
- ⁷⁰A. I. Tóth and G. Zaránd, *Phys. Rev. B* **78**, 165130 (2008).
- ⁷¹F. B. Anders, *Phys. Rev. B* **71**, 121101 (2005).
- ⁷²N. L. Dickens and D. E. Logan, *J. Phys. Condens. Matter* **13**, 4505 (2001).
- ⁷³M. R. Galpin, A. B. Gilbert, and D. E. Logan, *J. Phys. Condens. Matter* **21**, 375602 (2009).

- ⁷⁴In practice, T_K^{SC} is determined from a thermodynamic NRG calculation via $S_{\text{imp}}(T_K^{SC}) = \frac{1}{4} \ln(2)$, as such halfway between the characteristic 2CK and FL FP values.
- ⁷⁵J. M. Ziman, *Elements of Advanced Quantum Theory* (Cambridge University Press, Cambridge, 1995).
- ⁷⁶K. Chen and C. Jayaprakash, *Phys. Rev. B* **57**, 5225 (1998).
- ⁷⁷J. Schrieffer and P. Wolff, *Phys. Rev.* **149**, 491 (1966).
- ⁷⁸Y. Meir and N. S. Wingreen, *Phys. Rev. Lett.* **68**, 2512 (1992).
- ⁷⁹F. B. Anders, D. E. Logan, M. R. Galpin, and G. Finkelstein, *Phys. Rev. Lett.* **100**, 086809 (2008).
- ⁸⁰J. M. Maldacena and A. W. W. Ludwig, *Nucl. Phys. B* **506**, 565 (1997).
- ⁸¹G. Zaránd, L. Borda, J. von Delft, and N. Andrei, *Phys. Rev. Lett.* **93**, 107204 (2004).
- ⁸²L. Borda, L. Fritz, N. Andrei, and G. Zaránd, *Phys. Rev. B* **75**, 235112 (2007).